

---

# On the failure of variational score matching for VAE models

---

Li Kevin Wenliang\*

Gatsby Computational Neuroscience Unit  
University College London  
kevinli@gatsby.ucl.ac.uk

## Abstract

Score matching (SM) is a convenient method for training flexible probabilistic models, which is often preferred over the traditional maximum-likelihood (ML) approach. However, these models are less interpretable than normalized models; as such, training robustness is in general difficult to assess. We present a critical study of existing variational SM objectives, showing catastrophic failure on a wide range of datasets and network architectures. Our theoretical insights on the objectives emerge directly from their equivalent *autoencoding losses* when optimizing variational autoencoder (VAE) models. First, we show that in the Fisher autoencoder, SM produces far worse models than maximum-likelihood, and approximate inference by Fisher divergence can lead to low-density local optima. However, with important modifications, this objective reduces to a regularized autoencoding loss that resembles the evidence lower bound (ELBO). This analysis predicts that the modified SM algorithm should behave very similarly to ELBO on Gaussian VAEs. We then review two other FD-based objectives from the literature and show that they reduce to uninterpretable autoencoding losses, likely leading to poor performance. The experiments verify our theoretical predictions and suggest that only ELBO and the baseline objective robustly produce expected results, while previously proposed SM methods do not.

## 1 Introduction

Finding robust algorithms for training expressive latent variable models remains at the heart of unsupervised learning research. Latent variable models describe the data distribution by mapping a prior distribution of latent variables through a likelihood. A well-established approach for training such models is maximum likelihood (ML) that minimizes the Kullback-Leibler divergence (KLD) between the data and model distributions. Exact ML is usually intractable in practice; instead, one optimizes a lower bound of the log-likelihood (or upper bound on the KLD) defined through a variational distribution, known as the evidence lower bound (ELBO) [14, 23]. These approaches have produced robust results across task, datasets and model architectures [15]. Score matching offers another approach to training statistical models [12]; it minimizes the Fisher divergence (FD), a convenient objective for potentially unnormalized models. When latent variables are present, a situation we focus on here, the FD can be approximated [e.g. 27, 28, 2, 7].

Practitioners, who want to model their datasets under budget, see these two alternatives and naturally ask: which one is more robust so that the results are generally good without expensive hyperparameter search? KLD and FD are connected through differential relationships [26, 9, 18], but these results do not predict the robustness of using these divergences for training. Some previous work examined the difference between ML and SM in fully observed models [29, 1, 25] and latent variable models [2]; however, comparisons that control for the model class are missing. In addition, existing SM

---

\*Partially carried out during an internship at Amazon Web Services Shanghai Lablet.

objectives that give empirical success appear similar to each other [7, 2] but their differences remain unclear. Addressing these issues gives better understand of these methods, and avoid unexpected failures and expensive hyperparameter search. Further, a well-controlled comparison can reveal whether the improvements seen previously should be attributed to training objectives or other details.

Here, we conduct such a study of variational SM objectives using variational autoencoding models (VAEs) to unveil their differences and connection. Importantly, the joint distribution of a VAE model is normalized and thus can be trained conveniently via ML and SM; as such, VAE models provide an intuitive setup for theoretical analysis and well-controlled experiments: a robust ML or SM algorithm must be capable of training a VAE on a dataset. In particular, we focus on Gaussian VAEs on which important theoretical insights have been derived and practical successes seen [e.g. 5, 20, 4, 24].

In Section 2, we review the traditional variational ML approach and its objective (ELBO). **Our main contributions** consist of the analyses and illustrations in Sections 3 and 4, and the experiments in Section 5. Specifically, Section 3 studies a recently proposed variational SM objective known as the Fisher autoencoder [7]. We show that this objective can perform poorly in a counterintuitive way. We then, for the purpose of comparison, introduce a benchmark SM objective that is very similar to ELBO in their equivalent autoencoding losses and is thus expected to work as well as the latter. Unfortunately, two other existing SM objectives [27, 2] do not admit any reasonable autoencoding loss Section 4. Experiments (Section 5) demonstrate that the benchmark variational SM objective gives comparable performance to ELBO on several metrics, while the other variational objectives often failed. A concluding summary and limitations of this work are discussed in Section 6.

## 2 Background: variational autoencoders and maximum likelihood

We analyze training objectives on VAEs in which the generative model is expressed as  $p_\theta(z, x) = p(z)p_\theta(x|z)$ , where  $z \in \mathbb{R}^{d_z}$  is latent,  $x \in \mathbb{R}^{d_x}$  is observed, and  $\theta$  is the vector of parameters. The prior is fixed for the purpose of this study. The parameters  $\theta$  of this model is trained using i.i.d. samples of a dataset  $\mathcal{D}$  so that the marginal  $p_\theta(x) = \int p(z)p_\theta(x|z)dz$  is close to the underlying unknown data density  $\pi(x)$ . To find  $\theta$ , maximum-likelihood (ML) optimizes the marginal KLD  $\mathbb{D}_{\text{KL}}[\pi(x)||p_\theta(x)] := \mathbb{E}_\pi[\log \pi(x) - \log p_\theta(x)]$ , which is intractable for most models used in practice. A more practical approach to ML is to optimize ELBO:

$$\mathcal{F}_{q,\theta}(x) := \mathbb{E}_q[\log p_\theta(x|z)] - \mathbb{D}_{\text{KL}}[q(z|x)||p(z)], \quad (1)$$

where  $q(z|x)$  is a variational distribution in some prespecified distributional family  $\mathcal{Q}$ . It is usually parametrized by  $\phi$  which is independent of  $\theta$ . It can be shown that maximizing the expected ELBO amounts to minimizing the joint KLD

$$\mathbb{D}_{\text{KL}}[q(z|x)\pi(x)||p_\theta(z, x)] = \mathbb{E}_\pi[\mathbb{D}_{\text{KL}}[q(z|x)||p_\theta(z|x)]] + \mathbb{D}_{\text{KL}}[\pi(x)||p_\theta(x)]. \quad (2)$$

The joint KLD is attractive for learning  $\theta$  because it upper bounds the marginal KLD, and the variational posterior  $q$  can be optimized independently of  $\theta$ . In this work, we focus on the Gaussian VAE where the relevant densities are given by

$$p(z) = \mathcal{N}(0, I), \quad p_\theta(x|z) = \mathcal{N}(x; g_\theta(z), \gamma I), \quad q(z|x) = \mathcal{N}(z; \mu(x), \Sigma(x)). \quad (3)$$

Here, the functions  $g_\theta$ ,  $\mu$  and  $\Sigma$  specify the distribution parameters, and  $\gamma > 0$  is a scalar variance of the likelihood. In later sections, we sometimes relax the assumption that  $p(x)$  is Gaussian. The Gaussian VAE is not only widely used in practice for modelling complex continuous data distributions but also intuitive for deriving interesting properties. For example, it can be shown [6, 4] that in the limit of small posterior variance, the ELBO on the Gaussian VAE reduces to the following autoencoding objective at its optimum

$$\min_{\theta, q} h_{\text{K}} \left( \frac{1}{N} \sum_{n=1}^N \mathcal{L}_{\text{KL}, q, \theta}(x_n) \right) + \frac{1}{N} \sum_{n=1}^N \|\mu(x_n)\|_2^2, \quad (4)$$

$$\mathcal{L}_{\text{KL}, q, \theta}(x) := \|x - \mathbb{E}_q[g_\theta(z)]\|_2^2 + \sum_{j=1}^{d_x} \mathbb{V}_q[g_\theta(z)_j],$$

where  $h_{\text{K}}(y) := d_x \log(y/d_x)/2$  is an increasing concave function approaching  $-\infty$  as  $y \rightarrow 0_+$ . Importantly, Dai et al. [4] further showed that the unbounded gradient around zero in  $h$  is necessary for learning a form of *optimal sparse representation* of the data. Such a property is valuable to many downstream applications that rely on efficient lower-dimensional representations. We will see how the autoencoding loss (4) is related to objectives of variational score matching in Gaussian VAEs.

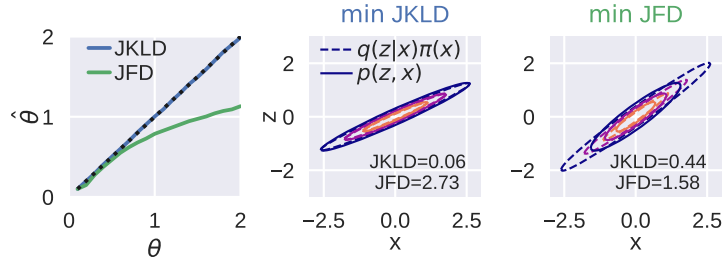


Figure 1: Parameter recovery by minimizing joint FD or joint KLD and the solutions. The bias in JFD minimization is substantial (left). For  $\theta = 2$ , minimizing the JKLD gave a more sensible solution (middle) than minimizing the JFD (right).

### 3 Variational score matching

As an alternative to ML, SM minimizes the marginal FD between the data and model distributions

$$\mathbb{D}_F[\pi(x)||p_\theta(x)] := \frac{1}{2} \mathbb{E}_\pi \left[ \|\nabla_x \log \pi(x) - \nabla_x \log p_\theta(x)\|_2^2 \right], \quad (5)$$

where  $\nabla_x$  is the Jacobian w.r.t.  $x$ . Practical algorithms for fully observed models were initially proposed by Hyvärinen [12]. Here, we consider SM algorithms for VAE models. For brevity, we define the following shorthands  $s_\theta^p(x|z) := \nabla_x \log p_\theta(x|z)$  and  $s^q(z|x) := \nabla_x \log q(z|x)$ .

#### 3.1 Revisiting Fisher autoencoder

As discussed in Section 2, the joint KLD (JKLD) provides a convenient objective for approximate ML. Elkhilil et al. [7] applied this intuition to SM and proposed the Fisher autoencoder (FAE) which optimizes the joint FD (JFD)

$$\mathbb{D}_F[q(z|x)\pi(x)||p_\theta(z,x)] = \mathbb{E}_\pi \{ \mathbb{D}_F[q(z|x)||p_\theta(z|x)] + J_{q,\theta}^\pi(x) \}, \quad (6)$$

$$J_{q,\theta}^\pi(x) := \frac{1}{2} \mathbb{E}_q \left\| \nabla_x \log \pi(x) + s^q(z|x) - s_\theta^p(x|z) \right\|_2^2 = \frac{1}{2} \mathbb{E}_q \left\| \nabla_x \log \frac{\pi(x)}{p_\theta(x)} + \nabla_x \log \frac{q(z|x)}{p_\theta(z|x)} \right\|_2^2. \quad (7)$$

A derivation is given in Appendix A.1. The two terms in (6) arise from the partial derivatives w.r.t.  $z$  and  $x$ , respectively. For a fixed  $\theta$ , if  $q(z|x) = p_\theta(z|x)$  for all  $x$  and  $z$ , then  $\mathbb{E}_\pi[J_{q,\theta}^\pi(x)] = \mathbb{D}_F[\pi(x)||p_\theta(x)]$ . Elkhilil et al. [7] further showed that  $\mathbb{E}_\pi[J_{q,\theta}^\pi(x)]$  is equal (up to a  $\pi$ -dependent constant that can be ignored for optimization) to  $\mathbb{E}_\pi[M_{1,q,\theta}(x)]$ , where

$$M_{1,q,\theta}(x) = \mathbb{E}_q \left[ \frac{1}{2} \|s_\theta^p(x|z)\|_2^2 + \nabla_x \cdot s_\theta^p(x|z) \right] + \frac{1}{2} \mathbb{E}_q \left[ \|s^q(z|x)\|_2^2 \right] \quad (8)$$

is a practical objective for SM. However, unlike the KLD case (2), the JFD is *not* an upper bound on the marginal FD. This means that a good fit over JFD may not imply a good fit over the target marginal FD. A perfect match in the joint distributions implies a perfect match on their marginals. But when the joint distributions do not match *exactly*, there is generally no guarantee that the marginals will be close, unless there is a bounding relationship as in the KLD case.

For example, consider a simple VAE defined by a prior  $p(z) = \mathcal{N}(0, 1)$ , likelihood  $p_\theta(x|z) = \mathcal{N}(\theta x, \gamma)$ , and a parametric variational posterior  $q_\phi(z|x) = \mathcal{N}(\phi x, \alpha v^*)$ , where  $v^* := (1 + \theta^2/\gamma)^{-1}$  is the exact posterior variance for the generative model,  $\gamma = 0.5$  is fixed, and the factor  $\alpha$  is used to impose posterior mismatch. Suppose we perform parameter recovery: Let the data distribution  $\pi$  be  $p_\theta$  for a ground truth  $\theta = \theta^*$ , and we wish to recover  $\theta^*$  by  $\min_{\phi,\theta} \mathbb{D}_F[q_\phi(z|x)\pi(x)||p_\theta(z,x)]$ . When  $\alpha = 1$ , the posterior is exact, and thus any setting of  $\theta^*$  can be recovered. We focus on the case where  $\alpha = 0.6$  and show that  $\hat{\theta}$  estimated by JFD minimization can be far away from  $\theta^*$  (Figure 1, left). On the contrary, minimizing the JKLD produced robust estimates. To further illustrate this problem, we plot  $q(z|x)\pi(x)$  and  $p_\theta(z,x)$  found by minimizing JKLD and JFD in Figure 1 when the true  $\theta = 2.0$ . These joints are close in JFD but not at all in JKLD or visual judgment. Therefore, minimizing JFD jointly over  $\theta$  and  $q$  [7] may be undesirable when  $q$  is approximate.

#### 3.2 Improved variational SM for semi-Gaussian VAEs

We took a closer look at the loss  $M_1$  proposed by Elkhilil et al. [7] and discovered that a simple modification can lead to an autoencoding loss similar to (4) for a wider class of VAEs. For a *semi-*

Gaussian VAE in which only the likelihood  $p_\theta(x|z) = \mathcal{N}(x; g_\theta(z), \gamma I)$  is Gaussian but  $p(z)$  and  $q(z|x)$  are unspecified, we have the following proposition, derived in Appendix A.2.

**Proposition 3.1.** *For a fixed  $q$ , the optimal semi-Gaussian VAE (3) that minimizes  $\mathbb{E}_{\mathcal{D}} [M_{1,\phi,\theta}(x)]$  solves the following autoencoding loss.*

$$\min_{\theta} h_{\mathbb{F}} \left( \frac{1}{N} \sum_{n=1}^N \mathcal{L}_{\text{KL},q,\theta}(x_n) \right), \quad \mathcal{L}_{\text{KL},q,\theta}(x) = \|x - \mathbb{E}_q[g_\theta(z)]\|_2^2 + \sum_{j=1}^{d_z} \mathbb{V}_q[g_\theta(z)_j], \quad (9)$$

where  $h_{\mathbb{F}}(y) = -d_x^2/(2y)$ , and  $\mathcal{L}_{\text{KL}}$  is repeated from (4).

*Remark 3.2.* The objective in (9) is almost identical to the first term in (4) derived from ELBO except for the utility function. Like  $h_{\mathbb{K}}$  in (4), the function  $h_{\mathbb{F}}$  in (9) is concave and has an unbounded gradient around zero, which is necessary for a sparse representation [4].

Proposition 3.1 suggests that  $M_1$  should in fact be used as an objective for optimizing  $\theta$  (learning) only, effectively removing the expectation under  $s^q$  in (8). On the other hand, the objective for optimizing  $q$  (inference) is unspecified. The rightmost equality in (7) indicates that if  $\nabla_x \log[q(z|x)/p_\theta(z|x)]$  is close to zero, then  $J_{q,\theta}^\pi(x)$  roughly equals the marginal FD. Therefore, a gradient step on  $\theta$  should not proceed until  $q$  closely matches  $p_\theta(z|x)$ . This overall procedure does not optimize the joint FD, as in FAE [7], or upper-bounds any marginal divergence; this is unlike variational ML which optimizes the joint KLD over  $q$  and  $\theta$  and bounds the marginal KLD from above. In practice, the variational  $q$  can be updated by FD or KLD, as discussed in the next subsection.

We stress the algorithm described above **does not optimize the joint FD as in FAE [7], nor does it perform coordinate descent between  $\theta$  and  $q$  on the original JFD**. In this procedure,  $M_1$  is used to optimize for  $\theta$  only, which effectively removes the second summand in the FAE objective (8); this term is also not involved in optimizing  $q$ . Further,  $\theta$  is not optimized through the posterior FD in (6). Our modification thus deviates from FAE in nontrivial ways.

### 3.3 Fisher divergence for inference

Training an encoder by minimizing the KLD is a popular approach for many VAE models and even jointly unnormalized models [2]. However, for real  $z$ , the FAE objective (6) suggests FD as an objective for inference. While both divergences can be estimated and optimized easily for the Gaussian VAE model, it is unclear which objective should be preferred for inference. Here, we discuss properties of the solution and optimization when  $q$  is optimized for FD.

#### 3.3.1 Optimal posterior in Gaussian VAEs

For a Gaussian VAE, in situations where the data have low noise (e.g. natural images), the optimal posterior usually has small variance. In this case, as explained in Appendix A.4, the posterior FD approximately reduces to

$$\mathbb{D}_{\mathbb{F}}[q(z|x)||p_\theta(z|x)] \approx \frac{1}{2} \|\mu^*(x)\|_2^2, \quad (10)$$

where the optimal posterior precision of  $q$  is  $\Lambda^* \approx I + \frac{1}{\gamma} (\nabla_z g_\theta(z) \nabla_z g_\theta(z)^\top)|_{\mu^*(x)}$ . As such, when the Gaussian VAE model is well trained and the posterior variance is small, FD as the inference objective regularizes the posterior mean in a way similar to the KLD (4). Further, the optimal  $\Lambda^*$  in FD coincides with that in KLD as derived by Dai et al. [5, Equation 83]. Thus, using FD for inference can produce the same desirable effects arising from this  $\Lambda^*$  discussed by the authors. However, Equation (10) also reveals that the optimal Gaussian  $q$  still incurs nonzero FD. The joint and marginal FDs in (6) are then separated by the nonzero posterior FD Equation (10). Therefore, we expected that FD is not an ideal inference objective for learning a Gaussian VAE by JFD or  $M_1$ .

#### 3.3.2 Local optima in FD optimization

Having characterized the solution of FD inference on a Gaussian VAE, we now turn to optimization. Elkhailil et al. [7] proposed to optimize a parametric  $q_\phi$  using the unbiased reparametrization gradient. However, we were unable to produce any reasonable results with this approach, which prompted us to investigate optimization on simpler problems. Consider a generative model with a standard Gaussian prior and a likelihood in

$$p_{\text{I}}(x = 2|z_1, z_2) = \mathcal{N}(x = 2; z_1 z_2, 0.5^2), \quad p_{\text{II}}(x = 1|z_1, z_2) = \mathcal{N}(x = 1; z_1 \text{relu}(z_2), 1.0^2). \quad (11)$$

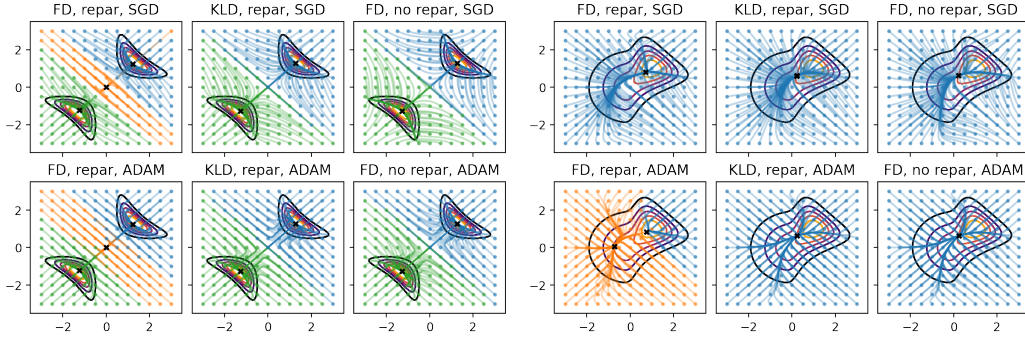


Figure 2: Optimizing a Gaussian  $q$  under a Gaussian prior and the simple likelihoods (11) by  $\mathbb{D}_{\text{KL}}$  and  $\mathbb{D}_{\text{F}}$  with or without reparametrization. Panels on the left is for  $p_{\text{I}}$ . The heat contours show the true posterior distributions. The regular grid of dots show the initial means of the Gaussian  $q$ ; the curved lines show the trajectories of the means during optimization that end at black crosses; The colors blue, green and orange are determined by the location of the mean on convergence.

---

**Algorithm 1:** Variational score matching, used as a benchmark for existing SM objectives.

---

**Input:** model  $p_{\theta}$ , variational  $q_{\phi}$ ,  $S$  posterior samples,  $J$  consecutive updates to  $q$

**while** not converged **do**

**for**  $k = 1, \dots, J$  **do**

    Update  $\phi \propto \nabla_{\phi} \mathbb{D}_{\text{KL}}[q_{\phi}(z|x)||p_{\theta}(z|x)]$  w/ repar., or  $\nabla_{\phi} \mathbb{D}_{\text{F}}[q_{\phi}(z|x)||p_{\theta}(z|x)]$  w/o repar.  
    estimated by  $S$  samples from  $q$ .

**end**

  Update  $\theta \propto \nabla_{\theta} M_{1,\phi,\theta}(x)$  (8) estimated by  $S$  samples from  $q$ .

**end**

---

The posteriors  $p_{\theta}(z|x)$  induced by these likelihoods as shown in Figure 2 (contours). To approximate these posteriors, we chose a variational family  $\mathcal{Q}$  as factorized Gaussians and optimized its mean and variance on  $\mathbb{D}_{\text{F}}[q_{\phi}(z|x)||p_{\theta}(z|x)]$  by either SGD or Adam [13], using reparametrization gradients. We visualize in Figure 2 (“FD, repar”) the trajectories of its mean when initialized at different points in the latent space. Surprisingly, for likelihood  $p_{\text{I}}$ , there is a low-density local optimum at the origin that attracts variational posteriors with means initialized from the orange dots. Using Adam exacerbated this problem by enlarging the basin of attraction. A similar issue also arises in the optimization of the Stein discrepancy [16]. In contrast, minimizing the KLD did not produce such a solution (“KLD, repar”). For the likelihood  $p_{\text{II}}$ , Adam also produced a local optima far away from the bulk of the posterior mass. SGD found a unique optimum regardless of initialization, but the solution was visibly different from that of KLD.

We hypothesize that the inappropriate convergence to low-density local optima is due to the gradient contribution of reparametrization: the FD can be lowered when  $q$  is driven to concentrate around a small region where its *shape* (but not its density) roughly matches the posterior’s (i.e.  $|\nabla_x \log p_{\theta}(z|x) - \nabla_z \log q(z|x)|$  is small). We test this hypothesis by optimizing  $q$  without reparametrization. In Appendix A.5.1, we show that the FD gradient without reparametrization is more similar to the KLD gradient than reparametrized gradient for a simple problem. Indeed, for the toy problems in Figure 2, following this gradient (“FD, no repar”) resulted in more similar dynamics and final solutions to KLD inference. More importantly, the posteriors no longer converge to the bad local optima. In our experiments on image data, we could only obtain a reasonable fit by using unparametrized gradients when FD was chosen as the objective. Although some advantage arises now that inference may not require reparametrized samples (Appendix A.5.2), this biased gradient can be problematic, such as when  $q$  is a Laplace (Appendix A.5.3).

Combining the results of FD-based learning and inference in Sections 3.2 and 3.3, we summarize the benchmark variational SM procedure in Algorithm 1. Since this algorithm is closely related to the ELBO (4), we expect their performances to be largely similar without hyperparameter tuning. Further practical limitations of Algorithm 1 are discussed in Section 6, and for these reasons, this

algorithm is used only to benchmark with other SM objectives in VAE models. It is also distinct from FAE [7] which failed badly in all our experiments.

## 4 Marginal SM objectives do not recover autoencoding losses

There are two closely related variational SM objectives [27, 2]. They optimize approximations to the marginal FD (5) rather than the joint FD, with implications that we discuss in detail here. First, Swersky et al. [27] derived an objective that is equivalent to (5) up to a  $\pi$ -dependent constant:

$$\mathbb{E}_\pi \left\{ \mathbb{E}_{p_\theta(z|x)} [\|s_\theta^p(x|z)\|_2^2 + \nabla_\theta \cdot s_\theta^p(x|z)] - \frac{1}{2} \|\mathbb{E}_{p_\theta(z|x)} [s_\theta^p(x|z)]\|_2^2 \right\}. \quad (12)$$

For a VAE model, one can replace  $p_\theta(z|x)$  with  $q$  in (12) to obtain a per-datum loss

$$M_{2,q,\theta}(x) := \mathbb{E}_q [\|s_\theta^p(x|z)\|_2^2 + \nabla_x \cdot s_\theta^p(x|z)] - \frac{1}{2} \|\mathbb{E}_q [s_\theta^p(x|z)]\|_2^2. \quad (13)$$

In the special case of Gaussian VAEs, we applied the same technique used for Proposition 3.1 to  $M_2$ , giving the following autoencoding loss.

**Proposition 4.1.** *The optimal semi-Gaussian VAE (3) that minimizes  $\mathbb{E}_D [M_{2,\phi,\theta}(x)]$  solves*

$$\min_{\theta,q} h_F \left( \frac{1}{N} \sum_{n=1}^N \mathcal{L}_{2,q,\theta}(x_n) \right), \quad \mathcal{L}_{2,q,\theta}(x) = \|x - \mathbb{E}_q [g_\theta(z)]\|_2^2 + 2 \mathbb{E}_q [\|g_\theta(z)\|_2^2]$$

where  $h_F(y) = -d_x^2/(2y)$ .

The second term of  $\mathcal{L}_2$  involves the expected  $\ell_2$  norm of the reconstruction mean, while the second term of  $\mathcal{L}_{KL}$  in (4) and (9) is the reconstruction variance. Thus, the objective proposed by Swersky et al. [27] applied to semi-Gaussian VAEs overly constrains the reconstruction.

Second, Bao et al. [2] inserted the identity  $\nabla_x \log p_\theta(x) = \mathbb{E}_{p_\theta(z|x)} [\nabla_x \log p_\theta(x|z)]$  into the marginal FD (5), giving

$$\mathbb{D}_F[\pi(x)||p_\theta(x)] = \frac{1}{2} \mathbb{E}_\pi \left[ \|\nabla_x \log \pi(x) - \mathbb{E}_{p_\theta(z|x)} [s_\theta^p(x|z)]\|_2^2 \right]. \quad (14)$$

The authors then replaced  $p_\theta(z|x)$  with a variational posterior  $q_\phi(z|x)$ . We derive its equivalent autoencoding loss below for semi-Gaussian VAEs.

**Proposition 4.2.** *Approximating  $p_\theta(z|x)$  with  $q(z|x)$ , the marginal FD (14) is equal to  $\mathbb{E}_\pi [M_{3,q,\theta}(x)]$ , up to a  $\pi$ -dependent constant, where*

$$M_{3,q,\theta}(x) := \mathbb{E}_q [s^q(z|x) \cdot s_\theta^p(x|z) + \nabla_x \cdot s_\theta^p(x|z)] + \frac{1}{2} \|\mathbb{E}_q [s_\theta^p(x|z)]\|_2^2. \quad (15)$$

In contrast to  $M_1$  and  $M_2$ , the autoencoding loss for  $M_3$  is not immediately interpretable and is deferred to Appendix A.2 only for completeness.

Another common issue of these two objectives above is that replacing the exact posterior with a variational  $q$  removes its dependence on  $\theta$ . Bao et al. [2] proposed to update  $\phi$  by  $\theta$ -dependent gradients. Nevertheless, this inner optimization is slow in practice and was discarded in the authors' main experiments. The contribution of this bi-level optimization is thus unclear, which we test empirically in Section 5. In contrast, the FAE based on the joint FD and Algorithm 1 based on our benchmark objective use a free variational posterior independent of  $\theta$ .

## 5 Experiments

To compare the effects of training objectives on Gaussian VAE models, we tested All combinations of the two inference objectives (KLD and FD) and the three SM objectives ( $M$ 's), yielding six overall SM objectives. The ELBO objectives is used as a baseline. Note that Bao et al. [2] used an objective that is equal to  $\mathbb{D}_{KL}-M_3$  in expectation. Optimizing FD with reparametrized gradient, or optimizing the joint FD as in Fisher autoencoder [7] did not give any reasonable results and are excluded for detailed comparison. The goal of these experiments is to confirm the analyses in previous sections. In particular, we expect that  $M_1$  is the only learning objective that can produce results similar to ELBO, and the other learning objectives are worse. Thus, we also do not expect the benchmark algorithm or any previous methods applied to VAEs to achieve state-of-the-art performance on any standard metrics. Details are in Appendix B and code is available at [github.com/kevin-w-li/LatentScoreMatching](https://github.com/kevin-w-li/LatentScoreMatching).

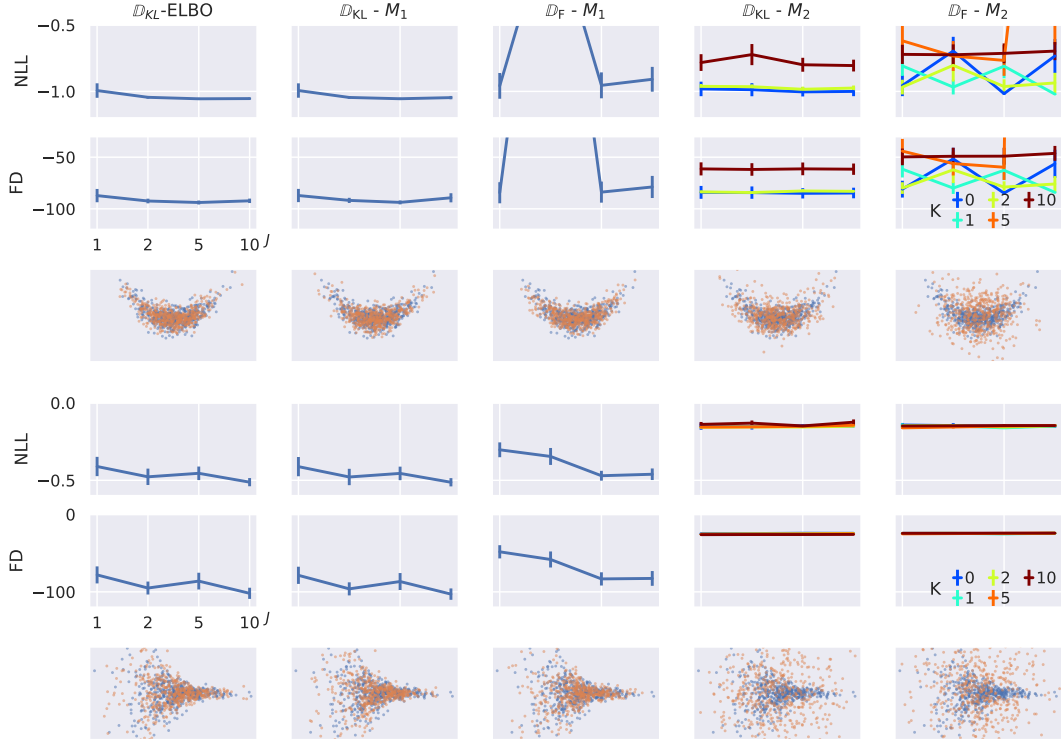


Figure 3: Results of models trained by different objectives (columns) on two sythetic datasets (top three and bottom three rows). We report the negative log likelihood and FD as we vary the number of independent encoder updates  $J$  and the number of bi-level encoder updates  $K$ , and samples from model with the lowest NLL (orange). Errorbar shows 1 sem from 10 independent initializations.

## 5.1 Synthetic datasets

We first trained Gaussian VAEs composed of fully connected layers (two hidden layers of 30 units) on simple 2D datasets. The latent space is  $\mathcal{R}^2$ . For each combined objective, we ran  $J \geq 1$  gradient updates to the encoder before updating the decoder. For objectives involving  $M_2$  and  $M_3$  where bi-level optimization is required, we also updated the encoder  $K \geq 0$  times with gradients that retain its dependence on  $\theta$ . The gradient for each update is computed using a minibatch of 1 000 samples. Each experimental setting is repeated 10 times. After training, the trained models are evaluated by the negative log-likelihood (NLL) and score matching loss (FD minus a constant) on unseen data, approximated by importance sampling using 100 000 samples.

The results are shown in Figure 3. The ELBO objective ( $\mathbb{D}_{\text{KL}}\text{-ELBO}$ ) and  $\mathbb{D}_{\text{KL}}\text{-}M_1$  produced almost equally good results, both the NLL and FD decrease as the number of encoder updates  $J$  increases, as expected. This confirms our analysis that these two objectives optimize very similar autoencoding losses. On the other had,  $\mathbb{D}_{\text{F}}\text{-}M_1$  is slightly worse, suggesting that the Fisher divergence is indeed not an ideal objective for learning  $\theta$ . The objectives involving  $M_2$  and  $M_3$  could not fit the model well. The NLL and FD for  $M_3$  objectives were above the limits of the figure axis ranges. On these two sythetic datasets, we did not observe strong positive effects of bi-level optimization. But we did observe this effect for much higher  $J$ ,  $K$  and network size; see Appendix B.1 where results on other sythetic datasets are also reported.

## 5.2 Benchmark datasets

**Procedure** We tested the variational SM on the Gaussian VAE model MNIST [17, CC BY-SA 3.0] and FashionMNIST [Fashion 30, MIT] and CelebA [19, CC-BY-4.0] datasets. All images are resized to  $32 \times 32$ . To avoid potentially unbounded gradients as  $\gamma \rightarrow 0$ , we added a small Gaussian noise to the data. This also prevented gross overfitting. Two neural architectures were tested: ConvNets as defined in DCGAN [21] and ResNets [10]. To ensure a good posterior approximation, we drew

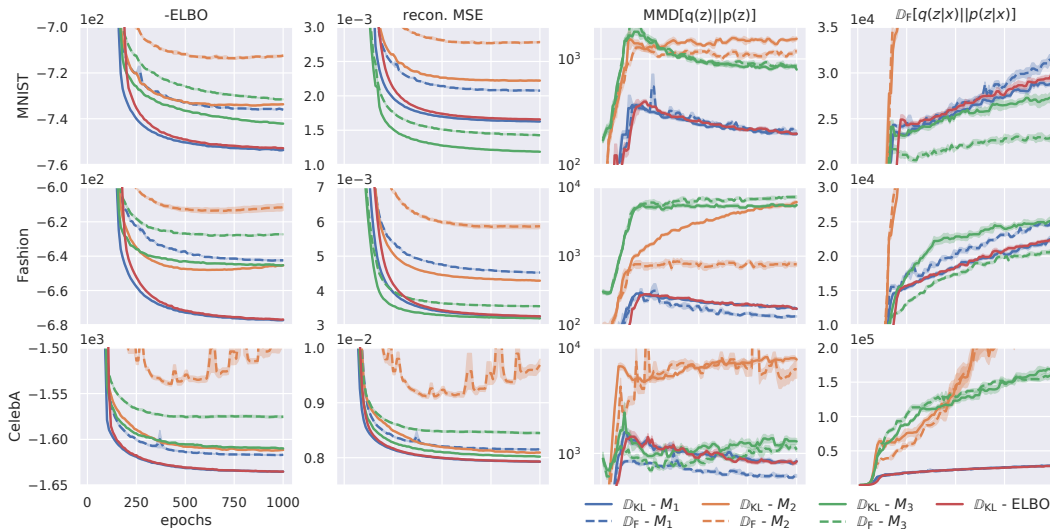


Figure 4: Test metrics (columns) for each dataset (rows). Lower is better. The objectives optimized is shown in the legend. The error bars are estimated based on 5 runs.

$S = 5$  samples from  $q$  to estimate expectations and updated  $q(z|x)$   $J = 5$  times for every  $\theta$  update. We did not perform bi-level optimization for large benchmark datasets [2]. Adam with step size  $10^{-4}$  was used as the optimization routine, and training lasted 1 000 epochs for each objective on each dataset. These experiments were run on NVIDIA<sup>®</sup> GTX 1080 GPUs.

To make a thorough comparison between the training objectives, we computed the following metrics on the test dataset after every 10 epochs: a) the **negative ELBO** as an overall metric; b) reconstruction mean squared error (**MSE**); c) the latent maximum mean discrepancy [**MMD**, 8] between the aggregate posterior  $q(z) := \int \pi(x)q(z|x)dx$  and  $p(z)$ , a global measure of the posterior approximation; and d) the **average FD** between the approximate and exact posteriors, a local measure of the posterior approximation. We also computed the **FID** [11] and **KID** [3], measuring sample quality, after training. Note that the latent MMD and the average posterior FD may increase through training as the true  $p_\theta(z|x)$  becomes more complicated.

**ConvNets** We focus on the results of ConvNets shown in Figure 4. The benchmark objective  $\mathbb{D}_{\text{KL}}-M_1$  gave learning trajectories almost identical to the  $\mathbb{D}_{\text{KL}}-\text{ELBO}$  on all metrics for all datasets.  $\mathbb{D}_{\text{F}}-M_1$  produced the best negative ELBO compared to the other  $\mathbb{D}_{\text{F}}$ - objectives but is still worse than  $\mathbb{D}_{\text{KL}}-\text{ELBO}$  or  $\mathbb{D}_{\text{KL}}-M_1$ . These are again consistent with our analyses. Comparing between the SM objectives, we found that  $M_2$  and  $M_3$  underperform  $\mathbb{D}_{\text{KL}}-\text{ELBO}$  and  $M_1$  on negative ELBO and latent MMD.  $M_2$  gave the highest reconstruction error, which may be the result of Proposition 4.1 that predicts over regularization of the reconstruction mean.  $M_3$  produced the lowest reconstruction MSE on the MNIST dataset only, but the latent MMD and posterior FD is large on other datasets.

Regarding inference,  $\mathbb{D}_{\text{F}}-M_1$  gave the lowest latent MMD on Fashion and CelebA, and  $\mathbb{D}_{\text{F}}-M_3$  gave the lowest posterior FD on CelebA. However, overall, methods with FD-based inference fared worse on latent MMD and posterior FD than those with  $\mathbb{D}_{\text{KL}}$ -based inference. Thus, KLD is indeed the preferred objective for variational learning even when the learning objective is FD, as done in Bao et al. [2]. The sample qualities are shown in Table 1.  $\mathbb{D}_{\text{KL}}+\text{ELBO}$  and the benchmark  $M_1$  gave some of the best FIDs. Again,  $\mathbb{D}_{\text{KL}}-M_1$  produced indistinguishable results compared to  $\mathbb{D}_{\text{KL}}+\text{ELBO}$ , but other objectives yielded worse FIDs.

**ResNets** So far, the empirical results are consistent across dataset, networks and different runs of the same settings. What if the VAE uses the more flexible ResNets? We focus on the sample quality metrics in (Table 1) and defer more detailed results to Appendix B.2.  $\mathbb{D}_{\text{KL}}-M_1$  produced better samples than  $\mathbb{D}_{\text{KL}}-\text{ELBO}$  on all datasets. The combination  $\mathbb{D}_{\text{F}}-M_1$  had better sample quality than  $\mathbb{D}_{\text{KL}}-M_1$  and  $\mathbb{D}_{\text{KL}}-\text{ELBO}$  (Table 1) on MNIST. Surprisingly, the best sample quality model turned out to be  $\mathbb{D}_{\text{F}}-M_2$ , although all  $\mathbb{D}_{\text{F}}$ - combinations produced the worst negative ELBO, reconstruction

Table 1: Sample quality ( $\text{KID} \times 10^3$ ) of model trained by different methods.  $\mathbb{K} := \mathbb{D}_{\text{KL}}$  and  $\mathbb{F} := \mathbb{D}_{\text{F}}$ .

Models	Objectives	ConvNets (5 runs, s.e $\leq 5\%$ )							ResNets		
		$\mathbb{K}$ -ELBO	$\mathbb{K}$ - $M_1$	$\mathbb{F}$ - $M_1$	$\mathbb{K}$ - $M_2$	$\mathbb{F}$ - $M_2$	$\mathbb{K}$ - $M_3$	$\mathbb{F}$ - $M_3$	$\mathbb{K}$ -ELBO	$\mathbb{K}$ - $M_1$	$\mathbb{F}$ - $M_1$
MNIST	FID	5.27	5.22	5.87	21.1	21.1	12.2	13.5	5.58	5.24	2.93
	KID	63.7	60.8	68.8	402	417	161	195	96.8	90.8	54.7
Fashion	FID	5.60	5.47	5.26	29.1	25.2	19.2	24.0	4.89	4.63	4.86
	KID	58.2	55.4	55.1	465	360	300	403	81.1	73.5	79.4
Celeb	FID	144	145	153	170	172	157	178	55.4	54.6	59.2
	KID	160	161	173	156	166	165	196	56.9	56.1	58.6

error and posterior FD than  $\mathbb{D}_{\text{KL}}$ - combinations (Appendix B.2). These results suggest strong effects of neural architecture on performance when  $M_2$  is used. In principle, using this objectives for training the decoder would require a bi-level optimization over  $q$ , but in practice this does not seem necessary when ResNets are used, as shown in the experiments here and previously [2].

**Sparse representation** Finally, to verify whether the objectives can produce sparse latent representation, we show the histogram of posterior standard deviation (SD) for each latent dimension in Appendix B.2, following Dai et al. [5]. For models with ResNet architecture, the posterior SDs trained by  $M_1$  are concentrated around either 0.0 or 1.0 (Figure 10), consistent with Remark 3.2. However, the same pattern is also observed on VAEs trained with the other learning objectives, even when the fit of the model is rather poor. Further, a sparse representation is also seen in a VAE model with binary latent variables Figure 11. Therefore, such a representation may be a more general phenomenon caused by factors that is not specific to ELBO or  $M_1$ . This sparse representation is less prominent using ConvNets Figure 9, especially on the more complex CelebA dataset.

## 6 Discussion

We performed an analytical and empirical comparison between existing score matching objectives [27, 2, 7]. Despite their excellent empirical results on image generation, the disparate model classes and training algorithms employed obscure the contributions from the training objectives. Here, we ask how these objectives perform in Gaussian VAEs that can be trained by maximum-likelihood and score matching. We found that minimizing the joint Fisher divergence [7] resulted in a significant bias in the learned distribution, but a simple modification gives rise to an objective  $M_1$  that resembles the ELBO on Gaussian VAEs. When combined with KLD-based inference, this objective yielded very similar performance with ELBO on different model architectures and datasets. Other learning objectives derived from the marginal Fisher divergence [27, 2] correspond to less effective autoencoding losses and require an expensive bi-level optimization in principle. They failed to learn simple synthetic datasets but appear more competent with more flexible neural architectures on real datasets. In addition, like the ELBO, the posterior FD can act as a regularizer on the encoded mean, but optimization on this objective can lead to poor local optima. In practice, KLD-based inference yielded better results over FD-based inference.

It is possible that our comparison ignored other important properties of these objectives. For example, the objectives that failed to perform well may have enormous estimation variances than the benchmark  $M_1$ , which resulted in less efficient learning in practice. Further, the benchmark algorithm has limitations that are worth mentioning. First, the learning objective  $M_1$  is not applicable to general jointly energy-based models. Second, the similarity between  $M_1$  and the ELBO may not be so obvious for non-Gaussian likelihoods; other SM objectives for certain likelihoods [22] may connect  $M_1$  and ELBO in more general cases. Despite these, our main message is clear: on the Gaussian VAE model, previous variational score matching algorithms often struggled to deliver satisfactory performance compared to variational maximum-likelihood or the benchmark score matching algorithm, which have more predictable behaviors. While this work does not in any way undermine the theoretical contributions made in those studies, it calls into question the contributions of their proposed *training objectives* to the empirical performances, and we cannot ignore the effects of detailed factors in the model and experiment.

## References

- [1] Michael Arbel and Arthur Gretton. “Kernel conditional exponential family”. In: *Artificial Intelligence and Statistics*. PMLR. 2018, pp. 1337–1346.
- [2] Fan Bao et al. “Bi-level score matching for learning energy-based latent variable models”. In: *Advances in Neural Information Processing Systems (2020)*.
- [3] Mikołaj Bińkowski et al. “Demystifying MMD GANs”. In: *International Conference on Learning Representations*. 2018.
- [4] Bin Dai, Li K Wenliang, and David Wipf. “On the Value of Infinite Gradients in Variational Autoencoder Models”. In: *Advances in Neural Information Processing Systems*. 2021.
- [5] Bin Dai and David Wipf. “Diagnosing and Enhancing VAE Models”. In: *International Conference on Learning Representations*. 2019.
- [6] Bin Dai et al. “Connections with robust PCA and the role of emergent sparsity in variational autoencoder models”. In: *The Journal of Machine Learning Research* 19.1 (2018), pp. 1573–1614.
- [7] Khalil Elkhilil et al. “Fisher Auto-Encoders”. In: *Artificial Intelligence and Statistics*. PMLR. 2021, pp. 352–360.
- [8] Arthur Gretton et al. “A kernel two-sample test”. In: *The Journal of Machine Learning Research* 13.1 (2012), pp. 723–773.
- [9] Dongning Guo. “Relative entropy and score function: New information-estimation relationships through arbitrary additive perturbation”. In: *2009 IEEE International Symposium on Information Theory*. IEEE. 2009, pp. 814–818.
- [10] Kaiming He et al. “Deep residual learning for image recognition”. In: *Proceedings of the IEEE conference on computer vision and pattern recognition*. 2016.
- [11] Martin Heusel et al. “GANs trained by a two time-scale update rule converge to a local nash equilibrium”. In: *Advances in Neural Information Processing Systems*. 2017, pp. 6629–6640.
- [12] Aapo Hyvärinen. “Estimation of non-normalized statistical models by score matching.” In: *Journal of Machine Learning Research* 6.4 (2005).
- [13] Diederik P Kingma and Jimmy Ba. “Adam: A Method for Stochastic Optimization”. In: *International Conference on Learning Representations*. 2015.
- [14] Diederik P Kingma and Max Welling. “Auto-Encoding Variational Bayes”. In: *International Conference on Learning Representations*. 2014.
- [15] D.P. Kingma and M. Welling. *An Introduction to Variational Autoencoders*. Foundations and trends in machine learning. 2019.
- [16] Anna Korba et al. “Kernel Stein Discrepancy Descent”. In: *International Conference on Machine Learning*. 2021.
- [17] Yann LeCun et al. “Gradient-based learning applied to document recognition”. In: *Proceedings of the IEEE* 86.11 (1998), pp. 2278–2324.
- [18] Qiang Liu and Dilin Wang. “Stein variational Gradient descent: a general purpose Bayesian inference algorithm”. In: *Advances in Neural Information Processing Systems*. 2016, pp. 2378–2386.
- [19] Ziwei Liu et al. “Deep Learning Face Attributes in the Wild”. In: *International Conference on Computer Vision*. 2015.
- [20] James Lucas et al. “Don’t blame the Elbo! a linear Vae perspective on posterior collapse”. In: *Advances in Neural Information Processing Systems* 32 (2019).
- [21] Alec Radford, Luke Metz, and Soumith Chintala. “Unsupervised representation learning with deep convolutional generative adversarial networks”. In: *arXiv preprint arXiv:1511.06434* (2015).
- [22] Martin Raphan et al. “Learning to be Bayesian without supervision”. In: *Advances in Neural Information Processing Systems* 19 (2007), p. 1145.
- [23] Danilo Jimenez Rezende, Shakir Mohamed, and Daan Wierstra. “Stochastic Backpropagation and Approximate Inference in Deep Generative Models”. In: *International Conference on Machine Learning*. 2014.
- [24] Oleh Rybkin, Kostas Daniilidis, and Sergey Levine. “Simple and effective vae training with calibrated decoders”. In: *International Conference on Machine Learning*. PMLR. 2021, pp. 9179–9189.

- [25] Yang Song et al. “Sliced score matching: A scalable approach to density and score estimation”. In: *Uncertainty in Artificial Intelligence*. PMLR. 2020, pp. 574–584.
- [26] Aart J Stam. “Some inequalities satisfied by the quantities of information of Fisher and Shannon”. In: *Information and Control* 2.2 (1959), pp. 101–112.
- [27] Kevin Swersky et al. “On autoencoders and score matching for energy based models”. In: *International Conference on Machine Learning*. 2011.
- [28] Eszter Vértés and Maneesh Sahani. “Learning doubly intractable latent variable models via score matching”. In: *Advances in Approximate Bayesian Inference*. 2016.
- [29] Li K Wenliang et al. “Learning deep kernels for exponential family densities”. In: *International Conference on Machine Learning*. PMLR. 2019, pp. 6737–6746.
- [30] Han Xiao, Kashif Rasul, and Roland Vollgraf. “Fashion-mnist: a novel image dataset for benchmarking machine learning algorithms”. In: *arXiv preprint arXiv:1708.07747* (2017).

# On the failure of variational score matching for VAE models: Supplementary material

## A Proofs and derivations

### A.1 FD between joint distributions

Starting from the joint Fisher divergence, we have

$$\begin{aligned}
\mathbb{D}_F[q(z|x)\pi(x)||p_\theta(z,x)] &:= \frac{1}{2}\mathbb{E}_{q\pi}\left[\left\|\nabla_{z,x}\log\frac{q(z|x)\pi(x)}{p_\theta(z)p_\theta(x|z)}\right\|_2^2\right] \\
&= \frac{1}{2}\mathbb{E}_{q\pi}\left[\left\|\nabla_z\log\frac{q(z|x)\pi(x)}{p_\theta(z)p_\theta(x|z)}\right\|_2^2 + \left\|\nabla_x\log\frac{q(z|x)\pi(x)}{p_\theta(z)p_\theta(x|z)}\right\|_2^2\right] \\
&= \frac{1}{2}\mathbb{E}_{q\pi}\left[\left\|\nabla_z\log\frac{q(z|x)\pi(x)}{p_\theta(z|x)p_\theta(x)}\right\|_2^2 + \left\|\nabla_x\log\frac{q(z|x)\pi(x)}{p_\theta(z|x)p_\theta(x)}\right\|_2^2\right] \\
&= \underbrace{\frac{1}{2}\mathbb{E}_{q\pi}\left[\left\|\nabla_z\log\frac{q(z|x)}{p_\theta(z|x)}\right\|_2^2\right]}_{\frac{1}{2}\mathbb{E}_\pi\mathbb{D}_F[q(z|x)||p_\theta(z|x)]} + \mathbb{E}_{q\pi}\left[\left\|\nabla_x\log\frac{\pi(x)}{p_\theta(x)} + \nabla_x\log\frac{q(z|x)}{p_\theta(z|x)}\right\|_2^2\right],
\end{aligned}$$

which is (6). The second line is obtained by separating the squared  $\ell_2$  norm of derivatives over  $z$  and  $x$  into two separate norms. The third line holds by applying the Bayes rule to the denominators in the logarithms. In the last line, we used the fact that  $\nabla_z\log p_\theta(x) = 0$  and  $\nabla_z\log\pi(x) = 0$ .

Thus, the joint FD decomposes into a sum of two terms that are, respectively, related to the partial derivatives w.r.t  $z$  and  $x$ . Below, we simplify the second term to get rid of the dependence on the unknown  $\nabla_x\log\pi(x)$ . One can show that the second term is equal to

$$J_{q,\theta}^\pi(x) := \mathbb{E}_{q(z|x)}\left[\left\|\nabla_x\log p_\theta(x|z) - \nabla_x\log q(z|x) - \nabla_x\log\pi(x)\right\|_2^2\right].$$

Then one has that

$$\begin{aligned}
\mathbb{E}_\pi[J_{q,\theta}^\pi(x)] &:= \frac{1}{2}\mathbb{E}_{q\pi}\left[\left\|\nabla_x\log p_\theta(x|z) - \nabla_x\log q(z|x) - \nabla_x\log\pi(x)\right\|_2^2\right] \\
&= \frac{1}{2}\mathbb{E}_{q\pi}\left[\left\|\nabla_x\log p_\theta(x|z)\right\|_2^2 + \left\|\nabla_x\log q(z|x)\right\|_2^2 + \left\|\nabla_x\log\pi(x)\right\|_2^2\right] \\
&\quad + \mathbb{E}_{q\pi}\left[\nabla_x\log q(z|x) \cdot \nabla_x\log\pi(x) - \nabla_x\log p_\theta(x|z) \cdot \nabla_x\log\pi(x)\right. \\
&\quad \left. - \nabla_x\log q(z|x) \cdot \nabla_x\log p_\theta(x|z)\right] \tag{16}
\end{aligned}$$

We will now simplify the first and second cross-terms (colored). The first one is zero. (The derivation by Elkhailil et al. [7] suggests that this term may be nonzero but depends only on  $\pi$ , which is an inconsequential error.)

$$\mathbb{E}_{q\pi}[\nabla_x\log q(z|x) \cdot \nabla_x\log\pi(x)] = \mathbb{E}_\pi[\mathbb{E}_{q(z|x)}[\nabla_x\log q(z|x)] \cdot \nabla_x\log\pi(x)] = 0.$$

The second cross-term of (16) is simplified as

$$\begin{aligned}
&\mathbb{E}_{q\pi}[\nabla_x\log p_\theta(x|z) \cdot \nabla_x\log\pi(x)] \\
&= \mathbb{E}_\pi[\mathbb{E}_{q(z|x)}[\nabla_x\log p_\theta(x|z)] \cdot \nabla_x\log\pi(x)] \\
&\stackrel{(1)}{=} -\mathbb{E}_\pi[\nabla_x \cdot \mathbb{E}_{q(z|x)}[\nabla_x\log p_\theta(x|z)]] \\
&\stackrel{(2)}{=} -\mathbb{E}_{q\pi}[\nabla_x\log q(z|x) \cdot \nabla_x\log p_\theta(x|z)] - \mathbb{E}_{q\pi}[\nabla_x \cdot \nabla_x\log p_\theta(x|z)],
\end{aligned}$$

where (1) follows from (25) and (2) uses the score trick. Substituting back to (16) cancels the blue term, and we arrive at  $\mathbb{E}_\pi \left[ \left\| J_{q,\theta}^\pi(x) \right\|_2^2 \right]$

$$\begin{aligned} &= \mathbb{E}_{q\pi} \left[ \frac{1}{2} \left\| \nabla_x \log p_\theta(x|z) \right\|_2^2 + \nabla_x \cdot \nabla_x \log p_\theta(x|z) + \frac{1}{2} \left\| \nabla_x \log q(z|x) \right\|_2^2 \right. \\ &\quad \left. + \frac{1}{2} \left\| \nabla_x \log \pi(x) \right\|_2^2 \right] \\ &= \mathbb{E}_\pi \left[ \underbrace{\mathbb{E}_q \left[ \frac{1}{2} \left\| \nabla_x \log p_\theta(x|z) \right\|_2^2 + \nabla_x \cdot \nabla_x \log p_\theta(x|z) + \frac{1}{2} \left\| \nabla_x \log q(z|x) \right\|_2^2 \right]}_{M_{1,q,\theta}(x)} + C_\pi \right]. \end{aligned}$$

where the  $\pi$ -dependent constant

$$C_\pi := \frac{1}{2} \left\| \mathbb{E}_{\pi(x)} [\nabla_x \log \pi(x)] \right\|_2^2, \quad (17)$$

## A.2 Autoencoding objectives for semi-Gaussian VAEs

Here, we show that the objectives  $M_1$  to  $M_3$  reduce to autoencoding objectives similar to (4) for semi-Gaussian VAEs where  $p(x|z) = \mathcal{N}(g_\theta(z), \gamma I)$ . We will use the following identities for semi-Gaussian VAEs extensively in our derivations

$$s_\theta^p(x|z) = -\frac{1}{\gamma}(x - g_\theta(z)) \quad (18)$$

$$\left\| \mathbb{E}_q [s_\theta^p(x|z)] \right\|_2^2 = \frac{1}{\gamma^2} \left\| x - \mathbb{E}_q [g_\theta(z)] \right\|_2^2 \quad (19)$$

$$\mathbb{E}_q \left[ \left\| s_\theta^p(x|z) \right\|_2^2 \right] = \frac{1}{\gamma^2} \mathbb{E}_q \left[ \left\| x - g_\theta(z) \right\|_2^2 \right] = \frac{1}{\gamma^2} \left[ \left\| x - \mathbb{E}_q [g_\theta(z)] \right\|_2^2 + \text{Tr } \mathbb{C}_q [g_\theta(z)] \right] \quad (20)$$

$$\nabla_x \cdot s_\theta^p(x|z) = -\frac{d_x}{\gamma} \quad (21)$$

In addition, one can check the following identity holds for any  $a > 0$  and  $b \in \mathbb{R}$

$$\min_\gamma \left\{ \frac{a}{2\gamma^2} - \frac{b}{\gamma} \right\} = -\frac{b^2}{2a} \quad (22)$$

**Proposition 3.1.** *For a fixed  $q$ , the optimal semi-Gaussian VAE (3) that minimizes  $\mathbb{E}_{\mathcal{D}} [M_{1,\phi,\theta}(x)]$  solves the following autoencoding loss.*

$$\min_\theta h_{\mathbb{F}} \left( \frac{1}{N} \sum_{n=1}^N \mathcal{L}_{\text{KL},q,\theta}(x_n) \right), \quad \mathcal{L}_{\text{KL},q,\theta}(x) = \left\| x - \mathbb{E}_q [g_\theta(z)] \right\|_2^2 + \sum_{j=1}^{d_z} \mathbb{V}_q [g_\theta(z)_j], \quad (9)$$

where  $h_{\mathbb{F}}(y) = -d_x^2/(2y)$ , and  $\mathcal{L}_{\text{KL}}$  is repeated from (4).

*Proof.* Since  $q$  is fixed,  $M_1$  is equal to the following up to a  $q$ -dependent constant

$$\begin{aligned}
\tilde{M}_{1,q,\theta}(x) &:= \mathbb{E}_q \left[ \frac{1}{2} \|s_\theta^p(x|z)\|_2^2 + \nabla_x \cdot s_\theta^p(x|z) \right] \\
&= \mathbb{E}_q \left[ \frac{1}{2\gamma^2} \left( \|x - \mathbb{E}_q[g_\theta(z)]\|_2^2 + \sum_{j=1}^{d_z} \mathbb{V}_q[g_\theta(z)_j] \right) \right] - \frac{d_x}{\gamma} \\
&= \frac{1}{2\gamma^2} \left\{ \|x - \mathbb{E}_q[g_\theta(z)]\|_2^2 + \sum_{j=1}^{d_z} \mathbb{V}_q[g_\theta(z)_j] \right\} - \frac{d_x}{\gamma} \\
\mathbb{E}_{\mathcal{D}} [\tilde{M}_{1,q,\theta}(x)] &= \frac{1}{2\gamma^2} \left\{ \frac{1}{N} \sum_{n=1}^N \|x_n - \mathbb{E}_{q(z|x_n)}[g_\theta(z)]\|_2^2 + \sum_{j=1}^{d_z} \mathbb{V}_{q(z|x_n)}[g_\theta(z)_j] \right\} - \frac{d_x}{\gamma}
\end{aligned}$$

The optimal VAE has an optimal  $\gamma$ . Using (22) to optimize out  $\gamma$ , we conclude that the optimal  $\theta$  is the solution to

$$h \left( \frac{1}{N} \sum_{n=1}^N \|x_n - \mathbb{E}_{q(z|x_n)}[g_\theta(z)]\|_2^2 + \sum_{j=1}^{d_z} \mathbb{V}_{q(z|x_n)}[g_\theta(z)_j] \right) \quad (23)$$

where  $h(y) = -d_x^2/(2y)$  □

**Proposition 4.1.** *The optimal semi-Gaussian VAE (3) that minimizes  $\mathbb{E}_{\mathcal{D}} [M_{2,\phi,\theta}(x)]$  solves*

$$\min_{\theta,q} h_{\mathbb{F}} \left( \frac{1}{N} \sum_{n=1}^N \mathcal{L}_{2,q,\theta}(x_n) \right), \quad \mathcal{L}_{2,q,\theta}(x) = \|x - \mathbb{E}_q[g_\theta(z)]\|_2^2 + 2 \mathbb{E}_q [\|g_\theta(z)\|_2^2]$$

where  $h_{\mathbb{F}}(y) = -d_x^2/(2y)$ .

*Proof.* We expand  $M_2$  using (18)-(21) as

$$\begin{aligned}
M_{2,q,\theta}(x) &:= \mathbb{E}_q [\|s_\theta^p(x|z)\|_2^2 + \nabla_x \cdot s_\theta^p(x|z)] - \frac{1}{2} \|\mathbb{E}_q[s_\theta^p(x|z)]\|_2^2 \\
&= \frac{1}{\gamma^2} \mathbb{E}_q [\|x - g_\theta(z)\|_2^2] - \frac{1}{2\gamma^2} \|x - \mathbb{E}_q[g_\theta(z)]\|_2^2 - \frac{d_x}{\gamma} \\
&= \frac{1}{2\gamma^2} \left\{ \|x - \mathbb{E}_q[g_\theta(z)]\|_2^2 + 2 \mathbb{E}_q [\|g_\theta(z)\|_2^2] \right\} - \frac{d_x}{\gamma} \\
\mathbb{E}_{\mathcal{D}} [M_{2,q,\theta}(x)] &= \frac{1}{N} \sum_{n=1}^N M_{2,q,\theta}(x_n) \\
&= \frac{1}{2\gamma^2} \left\{ \frac{1}{N} \sum_{n=1}^N \|x_n - \mathbb{E}_{q(z|x_n)}[g_\theta(z)]\|_2^2 + 2 \mathbb{E}_{q(z|x_n)} [\|g_\theta(z)\|_2^2] \right\} - \frac{d_x}{\gamma}
\end{aligned}$$

We then take the minimum w.r.t.  $\gamma$  and using (22) to obtain the loss

$$h \left( \frac{1}{N} \sum_{n=1}^N \|x_n - \mathbb{E}_{q(z|x_n)}[g_\theta(z)]\|_2^2 + 2 \mathbb{E}_{q(z|x_n)} [\|g_\theta(z)\|_2^2] \right) \quad (24)$$

where  $h(x) = -d_x^2/(2x)$  □

**Proposition A.1.** *The optimal semi-Gaussian VAE (3) that minimizes  $\mathbb{E}_{\mathcal{D}} [M_{3,\phi,\theta}(x)]$  is the solution to*

$$\begin{aligned} & \min_{\theta,q} h \left( \frac{1}{N} \sum_{n=1}^N \mathcal{L}_{3,q,\theta}(x_n) \right) \\ & \mathcal{L}_{3,q,\theta}(x) = g(\|x_n - \mathbb{E}_{q(z|x_n)} [g_{\theta}(z)]\|_2^2) \\ & g(x) = -\frac{1}{2x} \left( \frac{1}{N} \sum_{n=1}^N \mathbb{E}_q[s^q(z|x_n) \cdot (x_n - g_{\theta}(z))] + d_x \right)^2 \end{aligned}$$

*Proof.* We expand  $M_3$  using (19) and (21) as

$$\begin{aligned} M_{3,q,\theta}(x) & := \frac{1}{2} \|\mathbb{E}_q[s_{\theta}^p(x|z)]\|_2^2 + \mathbb{E}_q[s^q(z|x) \cdot s_{\theta}^p(x|z) + \nabla_x \cdot s_{\theta}^p(x|z)] \cdot \\ & = \frac{1}{2\gamma^2} \|x - \mathbb{E}_q[g_{\theta}(z)]\|_2^2 - \frac{1}{\gamma} (\mathbb{E}_q[s^q(z|x) \cdot (x - g_{\theta}(z))] + d_x) \\ \mathbb{E}_{\mathcal{D}} [M_{3,q,\theta}(x)] & = \frac{1}{2\gamma^2} \left\{ \frac{1}{N} \sum_{n=1}^N \|x_n - \mathbb{E}_q[g_{\theta}(z)]\|_2^2 \right\} \\ & \quad - \frac{1}{\gamma} \left\{ \frac{1}{N} \sum_{n=1}^N \mathbb{E}_q[s^q(z|x_n) \cdot (x_n - g_{\theta}(z))] + d_x \right\} \end{aligned}$$

We conclude the statement using (22). □

### A.3 Score matching objectives

We will use the following due to integration-by-parts when  $\pi(x) \rightarrow 0$  for sufficiently large  $x$ .

$$\begin{aligned} \mathbb{E}_{\pi(x)}[\nabla_x \log \pi(x) \cdot f(x)] & = \int \nabla_x \pi(x) \cdot f(x) dx = [\pi(x) \cdot f(x)]_{x \rightarrow -\infty}^{x \rightarrow \infty} - \mathbb{E}_{\pi(x)}[\nabla_x \cdot f(x)] \\ & = -\mathbb{E}_{\pi(x)}[\nabla_x \cdot f(x)] \end{aligned} \tag{25}$$

**Proposition 4.2.** *Approximating  $p_{\theta}(z|x)$  with  $q(z|x)$ , the marginal FD (14) is equal to  $\mathbb{E}_{\pi}[M_{3,q,\theta}(x)]$ , up to a  $\pi$ -dependent constant, where*

$$M_{3,q,\theta}(x) := \mathbb{E}_q[s^q(z|x) \cdot s_{\theta}^p(x|z) + \nabla_x \cdot s_{\theta}^p(x|z)] + \frac{1}{2} \|\mathbb{E}_q[s_{\theta}^p(x|z)]\|_2^2. \tag{15}$$

*Proof.* We expand (14) while approximating the posterior with  $q$ .

$$\begin{aligned} & \frac{1}{2} \mathbb{E}_{\pi(x)} [\|\nabla_x \log \pi(x) - \mathbb{E}_q[s_{\theta}^p(x|z)]\|_2^2] \\ & = \frac{1}{2} \mathbb{E}_{\pi(x)} [\|\mathbb{E}_q[s_{\theta}^p(x|z)]\|_2^2] - \mathbb{E}_{\pi(x)} [\nabla_x \log \pi(x) \cdot \mathbb{E}_{q(z|x)}[s_{\theta}^p(x|z)]] + \frac{1}{2} \|\mathbb{E}_{\pi(x)}[\nabla_x \log \pi(x)]\|_2^2 \\ & = \frac{1}{2} \mathbb{E}_{\pi(x)} [\|\mathbb{E}_q[s_{\theta}^p(x|z)]\|_2^2] + \mathbb{E}_{\pi(x)} [\nabla_x \cdot \mathbb{E}_{q(z|x)}[s_{\theta}^p(x|z)]] + C_{\pi} \\ & = \frac{1}{2} \mathbb{E}_{\pi(x)} [\|\mathbb{E}_q[s_{\theta}^p(x|z)]\|_2^2] + \mathbb{E}_{\pi(x)} \left[ \int \nabla_x q(z|x) \cdot s_{\theta}^p(x|z) dx + \mathbb{E}_q[\nabla_x \cdot s_{\theta}^p(x|z)] \right] + C_{\pi} \\ & \stackrel{(a)}{=} \mathbb{E}_{\pi(x)} \left[ \frac{1}{2} \|\mathbb{E}_q[s_{\theta}^p(x|z)]\|_2^2 + \mathbb{E}_{q(z|x)}[\nabla_x \log q(z|x) \cdot s_{\theta}^p(x|z) + \nabla_x \cdot s_{\theta}^p(x|z)] \right] + C_{\pi} \\ & = \mathbb{E}_{\pi(x)} [M_{3,q,\theta}(x)] + C_{\pi} \end{aligned}$$

where we have used the score approximator for the integral in equality (a). □

## A.4 Non-vanishing posterior fisher divergence in Gaussian VAEs

The Fisher divergence between the approximate and exact posterior is

$$\begin{aligned} & \mathbb{D}_F[q(z|x)||p_\theta(z|x)] \\ &= \int q(z|x) \|\nabla_z \log q(z|x) - \nabla_z \log p_\theta(z) - \nabla_z \log p_\theta(x|z)\|_2 dx dz \end{aligned}$$

For Gaussian VAEs, we substitute in the Gaussian densities in (3). To avoid unnecessary notational clutter, we will suppress the arguments to functions subscripts when no confusion arises.

$$\begin{aligned} \mathbb{D}_F[q(z|x)||p_\theta(z|x)] &= \int q(z|x) \left\| \Lambda(x)(z - \mu(x)) - z + \nabla_z g_\theta(z) \frac{x - g_\theta(z)}{\gamma} \right\|_2^2 dx dz \\ &= \int q(z|x) \|d_\theta(x, z)\|_2^2 dx dz \end{aligned} \quad (26)$$

where we have defined

$$d_\theta(x, z) := \Lambda(x)(z - \mu(x)) - z + \nabla_z g_\theta(z) \frac{x - g_\theta(z)}{\gamma} \quad (27)$$

Assume that the posterior will be relatively tight around the posterior mean  $\mu(x)$ , we expand the last term in the  $l$ -2 norm by Taylor expansion

$$\begin{aligned} \nabla_z g_\theta(z)(x - g_\theta(z)) &= [\nabla_z g_\theta(z)(x - g_\theta(z))]_\mu + \nabla_z [\nabla_z g_\theta(z)(x - g_\theta(z))]_\mu (z - \mu) + o(z^2) \\ &= \nabla_z g_\theta(z)|_\mu (x - g_\theta(\mu)) \\ &\quad + [\nabla_z \nabla_z g_\theta(z)(x - g_\theta(\mu)) - (\nabla_z g_\theta(z) \nabla_z g_\theta(z)^\top)|_\mu] (z - \mu) \\ &\quad + o_2((z - \mu)), \end{aligned}$$

where  $o_2(x)$  denotes terms that are 2nd or higher order in  $x$ . When the model has been trained to describe the data manifold by the latent space,  $\mu$  and  $g_\theta$  are inverse of one another, then  $x - g_\theta(\mu(x)) = 0$ , we have

$$\nabla_z g_\theta(z) \frac{x - g_\theta(z)}{\gamma} = - \frac{1}{\gamma} \underbrace{(\nabla_z g_\theta(z) \nabla_z g_\theta(z)^\top)|_{z=\mu(x)}}_{G_\theta(x)} (z - \mu(x)) + o_2(z - \mu).$$

Inserting this into the  $l$ -2 norm of (27) gives

$$\begin{aligned} d_\theta(x, z) &= \Lambda(x)(z - \mu(x)) - z - G_\theta(x)(z - \mu(x)) + o(z^2) \\ &= [\Lambda(x) - I - G_\theta(x)] z - [\Lambda(x) - G_\theta(x)] \mu(x) + o_2(z - \mu). \end{aligned}$$

Since  $z \sim q(z|x)$ , we can rewrite  $z = \mu(x) + \Lambda(x)^{-\frac{1}{2}} \epsilon$ , where  $\epsilon \sim \mathcal{N}(0, I)$ , which gives

$$d_\theta(x, z) = -\mu(x) + [\Lambda(x) - I - G_\theta(x)] \Lambda(x)^{-\frac{1}{2}} \epsilon + o_2(\Lambda(x)^{-\frac{1}{2}} \epsilon).$$

Inserting this back to (26) gives

$$\begin{aligned} \mathbb{D}_F[q(z|x)||p_\theta(z|x)] &\approx \|\mu(x)\|_2^2 \\ &\quad + \text{Tr} [(\Lambda(x) - I - G_\theta(x)) \Lambda(x)^{-1} (\Lambda(x) - I - G_\theta(x))]. \end{aligned}$$

Using standard multivariate calculus, it is straightforward to show that the last term reaches the minimum of 0 when  $\Lambda = I + G_\theta(x)$ . (The other solution  $\Lambda = -(I + G_\theta(x))$  is not positive-semidefinite.)

## A.5 Issues of Fisher divergence in inference

### A.5.1 Unparametrized FD gradients can resemble KLD gradients

Here, we compare the gradients of KLD and FD between two univariate Gaussian distributions. For FD, we will also compute the expression for the biased gradient obtained using unparametrized samples.

Consider two Gaussians defined as

$$p_1(x) = \mathcal{N}(x; m_1, s_1^2), \quad p_2(x) = \mathcal{N}(x; m_2, s_2^2), \quad (28)$$

And our goal is to optimize  $p_1$  to be close to  $p_2$ . The KLD between them is

$$\begin{aligned} \mathbb{D}_{\text{KL}}[p_1 \| p_2] &= \int q(x) \log \frac{q(x)}{p(x)} dx \\ &= -\frac{1}{2} \int p_1(x) \left[ \frac{(x - m_1)^2}{s_1^2} + \log(2\pi s_1^2) - \frac{(x - m_2)^2}{s_2^2} - \log(2\pi s_2^2) \right] dx \\ &= -\frac{1}{2} \left[ \frac{s_1^2}{s_1^2} + \log(2\pi s_1^2) - \frac{m_1^2 + s_1^2 - 2m_1m_2 + m_2^2}{s_2^2} - \log(2\pi s_2^2) \right] \\ &= -\frac{1}{2} \left[ 2 \log \left( \frac{s_1}{s_2} \right) - \frac{(s_1^2 - s_2^2) + (m_1 - m_2)^2}{s_2^2} \right] \end{aligned}$$

To optimize the KL w.r.t  $m_1$  and  $s_1$ , we can compute the gradients as

$$\frac{\partial}{\partial m_1} \mathbb{D}_{\text{KL}}[p_1 \| p_2] = \frac{m_1 - m_2}{s_2^2}, \quad \frac{\partial}{\partial s_1} \mathbb{D}_{\text{KL}}[p_1 \| p_2] = \frac{s_1^2 - s_2^2}{s_1 s_2^2}. \quad (29)$$

We now derive the expression for the FD gradient. Starting from the FD itself:

$$\begin{aligned} \mathbb{D}_{\text{F}}[p_1 \| p_2] &= \int q(x) \left| \frac{d}{dx} \log q(x) - \frac{d}{dx} \log p(x) \right|^2 dx \\ &= \int q(x) \left| \frac{x - m_1}{s_1^2} - \frac{x - m_2}{s_2^2} \right|^2 dx \\ &= \int q(x) \left[ \frac{(x - m_1)^2}{s_1^4} - \frac{2(x - m_1)(x - m_2)}{s_1^2 s_2^2} + \frac{(x - m_2)^2}{s_2^4} \right] dx \\ &= \frac{s_1^2}{s_1^4} - 2 \frac{m_1^2 + s_1^2 - m_1^2 - m_1 m_2 + m_1 m_2}{s_1^2 s_2^2} + \frac{m_1^2 + s_1^2 - 2m_1 m_2 + m_2^2}{s_2^4} \\ &= \frac{1}{s_1^2} - \frac{2}{s_2^2} + \frac{s_1^2 + (m_1 - m_2)^2}{s_2^4}. \end{aligned} \quad (30)$$

Then the derivatives w.r.t  $m_1$  and  $s_1$  are

$$\frac{\partial}{\partial m_1} \mathbb{D}_{\text{F}}[p_1 \| p_2] = \frac{2(m_1 - m_2)}{s_2^4}, \quad \frac{\partial}{\partial s_1} \mathbb{D}_{\text{F}}[p_1 \| p_2] = \frac{2(s_1^4 - s_2^4)}{s_1^3 s_2^4}. \quad (31)$$

Finally, we derive the biased gradient that ignores the dependency on the parameters through the  $q$  over which the expectation (30) is computed. This can be done by evaluating the parameter derivatives first before taking the expectation.

$$\nabla_v^b \mathbb{D}_{\text{F}}[p_1 \| p_2] := \int q(x) \nabla_v d(x) dx, \quad v \in \{m_1, s_1\}$$

$$d(x) := \left| \frac{d}{dx} \log q(x) - \frac{d}{dx} \log p(x) \right|^2 = \frac{x - m_1}{s_1^2} - \frac{x - m_2}{s_2^2}$$

$$\frac{\partial}{\partial m_1} d(x) = -\frac{2}{s_1^2} \left[ \frac{x - m_1}{s_1^2} - \frac{x - m_2}{s_2^2} \right] \quad \frac{\partial}{\partial s_1} d(x) = -\frac{4(x - m_1)}{s_1^3} \left[ \frac{x - m_1}{s_1^2} - \frac{x - m_2}{s_2^2} \right]$$

Now we evaluate the expectations to get

$$\frac{\partial^b}{\partial m_1} \mathbb{D}_{\text{F}}[p_1 \| p_2] = \frac{2(m_1 - m_2)}{s_1^2 s_2^2} \quad \frac{\partial^b}{\partial s_1} \mathbb{D}_{\text{F}}[p_1 \| p_2] = \frac{4(s_1^2 - s_2^2)}{s_1^3 s_2^2} \quad (32)$$

Thus, combining (29), (31) and (32), we have

$$\begin{aligned} \frac{\partial}{\partial m_1} \mathbb{D}_F[p_1 \| p_2] &= \frac{2}{s_2^2} \frac{\partial}{\partial m_1} \mathbb{D}_{\text{KL}}[p_1 \| p_2], & \frac{\partial}{\partial s_1} \mathbb{D}_F[p_1 \| p_2] &= \frac{2}{s_1^2 s_2^2} \frac{\partial}{\partial s_1} \mathbb{D}_{\text{KL}}[p_1 \| p_2]; \\ \frac{\partial^b}{\partial m_1} \mathbb{D}_F[p_1 \| p_2] &= \frac{2}{s_1^2} \frac{\partial}{\partial m_1} \mathbb{D}_{\text{KL}}[p_1 \| p_2], & \frac{\partial^b}{\partial s_1} \mathbb{D}_F[p_1 \| p_2] &= \frac{4}{s_1^2} \frac{\partial}{\partial s_1} \mathbb{D}_{\text{KL}}[p_1 \| p_2]. \end{aligned}$$

The biased FD gradient is equal to the KLD gradient up to a factor  $\propto s_1^{-2}$ . The unbiased gradient is also a scaled version of the KLD gradient, but the scaling factor depends on both  $s_1$  and  $s_2$ .

This analysis can be generalized to non-Gaussian  $p_2$ , such as arbitrary exponential family distributions. However, the final gradients depend on the derivatives of the sufficient statistics of  $p_2$ , which produces a less interpretable result once taken expectation over  $q_1$ .

### A.5.2 Fitting mixtures distributions to intractable posteriors

For the posteriors induced by the toy distributions, we can optimize Gaussian mixture distributions with 10 Gaussian components to minimize the FD, following the biased gradient computed through unparametrized samples drawn from the Gaussian mixture model. If instead we want to optimize w.r.t KLD, then one needs to reparametrize the discrete latent variable. We initialized the Gaussian components so that the means are random samples from the prior and the standard deviations are 1.0. The mixing proportions were initialized equal. All parameters are optimized using Adam with step size 0.001. 10 samples from the mixture was used to approximate the FD at each iteration, for a total of 5 000 iterations.

To test for robustness and reliability of this method, we ran the algorithm 10 times with different initializations. The results are shown in Figure 5. The posterior induced by  $p_I$  in (11), are bimodal with disjoint supports, so the fit can have arbitrary weighting between them, an issue known for many score-based methods. The fit for the posterior induced by  $p_{II}$  was much more stable across different runs.

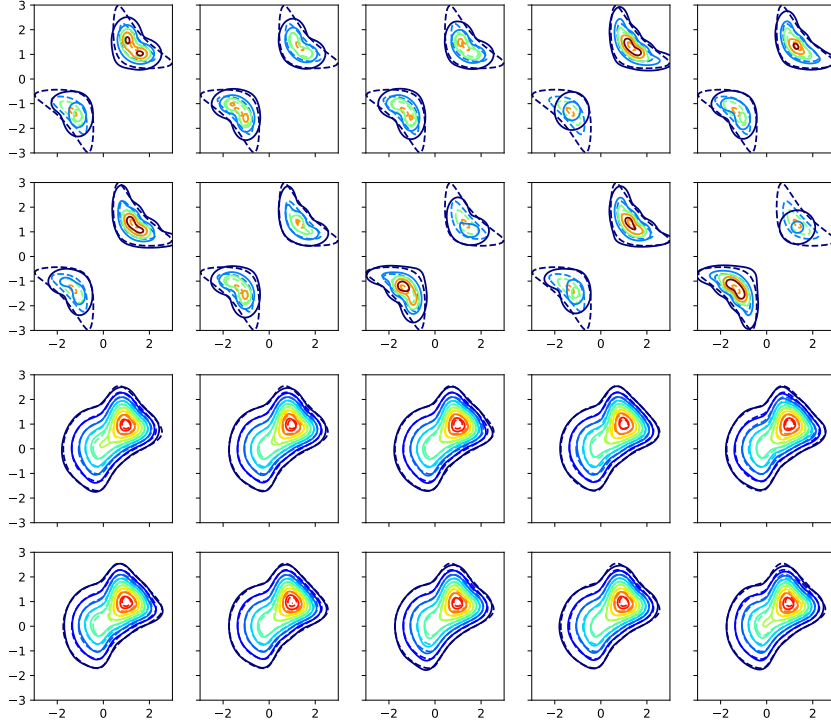


Figure 5: Fitting a Gaussian mixture distribution to posteriors induced by the likelihoods (11). Each panel is a run with a different initialization. Dashed line is the exact posterior approximated using histograms, and the solid lines are the model fit.

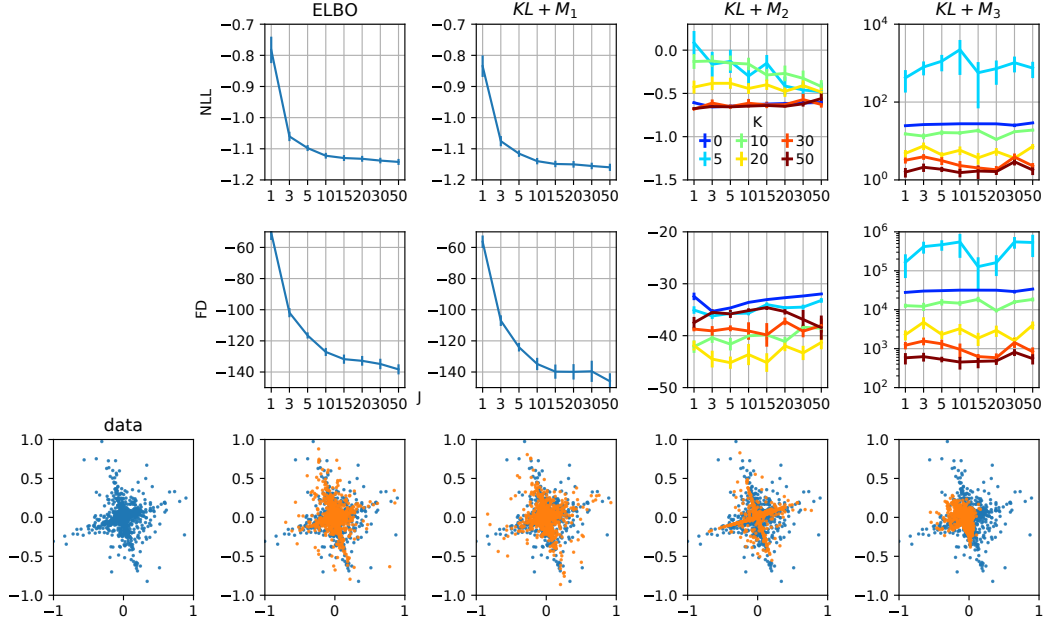


Figure 6: Test negative log-likelihood (top row) and Fisher divergence (middle row) of models trained on the star dataset. Note the different scales on the vertical axes. Bottom, generated and real samples of the model with the highest test log-likelihood.

### A.5.3 Fitting Laplace posterior with unparametrized samples

The Laplace distribution  $\text{Lap}(x; m, s)$  has a density function

$$\text{Lap}(x) \propto \exp\left(-\frac{|x - m|}{s}\right),$$

and its score function is independent of the mean  $m$  almost surely

$$\frac{\partial}{\partial x} \log \text{Lap}(x) = \begin{cases} +\frac{1}{s} & x < m, \\ -\frac{1}{s} & x > m. \end{cases}$$

and the biased gradient will be zero for  $m$ . Using the unbiased gradient becomes crucial for learning  $m$ .

## B Experiment details

### B.1 Details and extended results on synthetic datasets

As discussed in Section 4, the objectives  $M_2$  and  $M_3$  adapted from previous work yield a biased gradient when the  $\theta$ -dependent exact posterior is replaced by a variational approximation. To address this issue, Bao et al. [2] proposed a bi-level optimization technique to address the issue. Briefly, given one minibatch of data, before each  $\theta$  update (learning), the variational parameters  $\phi$  are updated with  $J$  ordinary gradient steps followed by  $K$   $\theta$ -parametrized gradient steps. For  $K > 0$ , this effectively makes  $\phi$  a function of  $\theta$ . Differentiating the resulting objective w.r.t.  $\theta$  then gives a less biased gradient. However, Bao et al. [2] set  $K =$  for their large-scale experiments, showing that this may not be necessary. Here, we empirically test the effect of  $K$  on simpler datasets and neural architectures for interpretability.

In the main text, we show the results of training with various objectives on two datasets in Figure 3. We repeated the same experiment on three additional datasets, and all results are collectively shown in Figure 7. In those experiments, we used 30 neurons for each of the two hidden layers in the VAE model. We show in Figure 6 the results on one dataset when using a larger network (two layers

of 100 hidden units), and larger values of  $J$  and  $K$  and longer training epochs (1 000). Here, we see that optimizing by *ELBO* and  $\mathbb{D}_{\text{KL}} + M_1$  produced very similar results with the latter being better. In addition, for  $M_2$  and  $M_3$ , the number of bi-level updates  $K$  had a substantial effect on NLL and FD. Nonetheless, the trained models were still much worse than *ELBO* and  $\mathbb{D}_{\text{KL}} + M_1$ . Thus, we reproduced the benefits of bi-level optimization, but these objectives still fail to fit the VAE model to this simple data set.

## B.2 Extended results on benchmark datasets

The latent space is  $\mathbb{R}^{100}$ , and the images are resize to  $32 \times 32$  (zero padding for MNIST and Fashion). The function  $g_\theta$  is a neural network with DCGAN architecture and ReLU nonlinearity<sup>2</sup>. The training batch size is 100. We used Adam with a step size of 0.0001 for variational methods, trained for 1000 epochs. We added a small isotropic Gaussian noise with sd 0.1 to the images. This is done for two reasons: 1) training with clean images or smaller std produced visible traits of overfitting on the test metrics; 2) noise stabilizes training as  $\gamma \rightarrow 0$ ;

For each variational algorithm, we draw  $S = 5$  samples from  $q$  (reparametrized for KLD inference and unparametrized for FD inference) to approximate the expectations in  $M_1$  to  $M_3$ . The encoder is updated for  $K = 5$  consecutive iterations on independent minibatches for every decoder update. We found this training procedure helped stabilize the training trajectories produced by all methods, including *ELBO*.

To evaluate the model on the test data, we computed

- reconstruction MSE: encode a noisy image, decode from the mean of  $q$ , and then compute the mean squared error averaged over test input and the dimensionality of  $x$ .
- the aggregate posterior MMD: draw one sample from  $q$  for each test image, then compute the MMD with samples from  $p(z)$ . We used a cubic kernel.
- posterior FD: we approximate  $\mathbb{D}_{\text{F}}[q(z|x)||p_\theta(z|x)]$  by 5 posterior samples, then average over all test  $x$ .
- negative *ELBO*: the reconstruction error is estimated by 5 samples from  $q$ , and the KL penalty is closed-form.

**Distribution of posterior standard deviation** To verify FD-based inference has the ability to obtain minimal latent representation implied in Section 3.3, we show the distribution of posterior standard deviations for all methods and distributions in Figure 9. It is clear that the standard deviations are concentrated around 0 and 1 on the MNIST dataset, consistent with the analysis in Section 3.3.

**Experiments on ResNet18** To test whether the observations so far hold for other network architectures, we ran the variational SM objectives and *ELBO* on VAE models with ResNet18<sup>3</sup>. Here, we set  $J = 1$  and  $S = 1$ . Again, KL-based inference gave better metrics on all the four measures. The performance metrics are shown in Figure 8, averaged over five runs. Again  $\mathbb{K} + M_1$  performed almost identical to *ELBO*, but now  $\mathbb{D}_{\text{KL}} + M_2$  and  $\mathbb{D}_{\text{KL}} + M_3$  also became similar to those two. This was not the case for the fully connected networks on synthetic datasets or convnets on benchmark dataset. Therefore, the network architecture seems to allow  $M_2$ - and  $M_3$ -based methods to improve quite substantially.

On sample quality, shown in Appendix B.2,  $M_2$  gave the best qualities while  $M_3$  were the worst. A notable difference is that Objectives with FD-based inference could lead to better sample quality. Objectives with FD-based inference can lead to better sample quality than those with KLD-based inference, although the *ELBO* or posterior quality were worse Figure 10. The histograms of posterior sds Figure 10 become more concentrated around 0 and 1 using ResNets than using ConvNets for all objectives, suggesting better capture of the data manifold by the latent codes in ResNet models.

**Experiments on binary latent variables** To test whether the minimal representation does not rely on a Gaussian prior, we trained a VAE model with binary  $z \in \{0, 1\}^{30}$ . We used a factorized Bernoulli  $q$  whose parameters are optimized by Gumble Softmax.

<sup>2</sup>Code taken from [pytorch.org/tutorials/beginner/dcgan\\_faces\\_tutorial.html](https://pytorch.org/tutorials/beginner/dcgan_faces_tutorial.html)

<sup>3</sup>Code taken from [github.com/julianstastny/VAE-ResNet18-PyTorch](https://github.com/julianstastny/VAE-ResNet18-PyTorch).

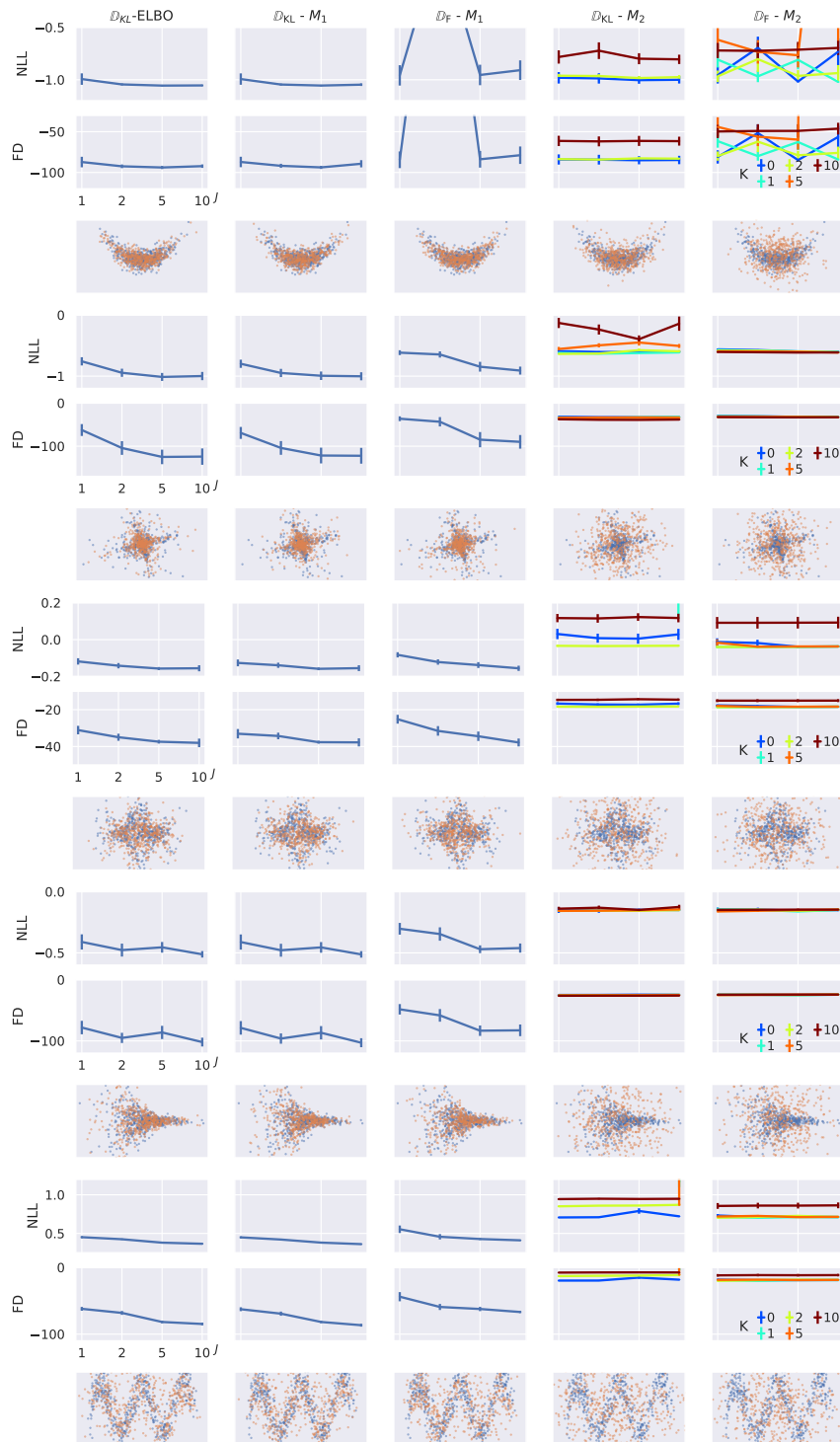


Figure 7: Same as Figure 3 but for all five synthetic datasets.

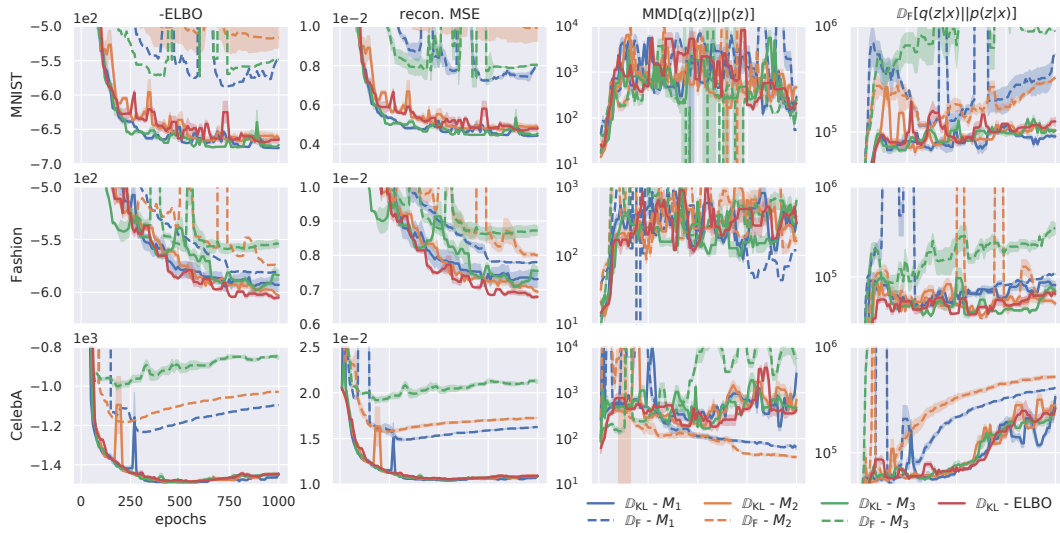


Figure 8: Same as Figure 4 but for VAE models with ResNet18 structure.

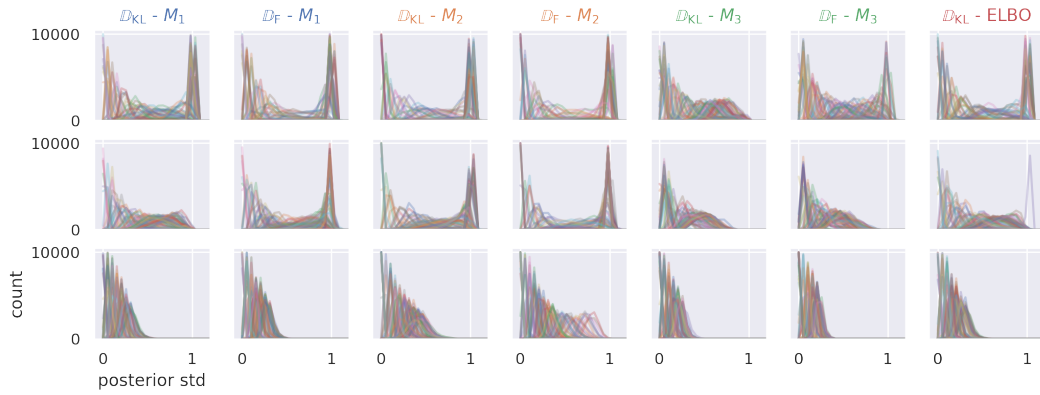


Figure 9: Histogram of posterior variance of each dimension (colored pale lines) and averaged over 100 dimension (black) for model with DCGAN network architecture.

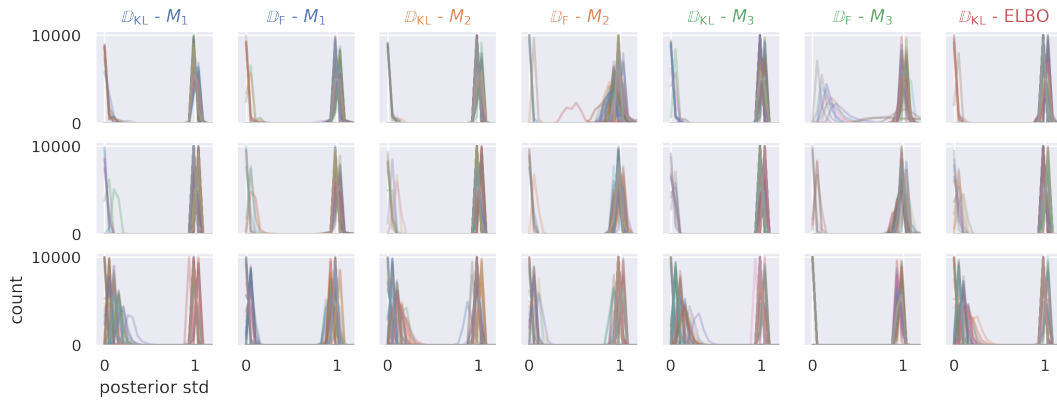


Figure 10: Same as Figure 9 but using models with ResNet architecture.

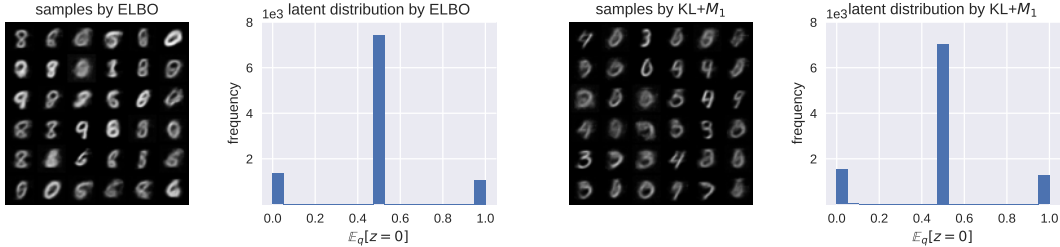


Figure 11: Results of a VAE with binary latent variables, trained by  $\mathbb{D}_{\text{KL}}$ -ELBO (left two panels) and  $\mathbb{D}_{\text{KL}}-M_1$  (right two panels). For each objective, we show the generated samples and the distributions of variational posterior mean conditioned on test data samples.

Table 2: Sample quality (KID  $\times 1000$ ) for variational models trained with ResNet18 architecture. Lower is better. Bold indicates the best.

Method	MNIST		Fashion		CelebA	
	FID	KID	FID	KID	FID	KID
Baseline						
VAE	5.58	96.8	4.89	81.1	55.4	56.9
Variational						
$\mathbb{K}+M_1$	5.24	90.2	4.63	73.5	54.6	56.1
$\mathbb{F}+M_1$	2.93	54.7	4.86	79.4	59.2	58.6
$\mathbb{K}+M_2$	5.81	99.8	4.77	76.0	<b>54.3</b>	<b>55.1</b>
$\mathbb{F}+M_2$	<b>2.88</b>	<b>44.3</b>	<b>3.65</b>	<b>52.2</b>	60.4	60.0
$\mathbb{K}+M_3$	12.6	264	10.7	205	208	226
$\mathbb{F}+M_3$	8.70	177	28.6	637	203	196

If a given dataset requires only a few latent codes to describe, then the redundant latent space will have their posteriors match the prior. In Figure 11, we see that is the case when the VAE model is trained by ELBO or  $\mathbb{D}_{\text{KL}}+M_1$ . The histograms show the distributions of the posterior means. Many of the latent dimensions have mean 0.5, suggesting that these dimensions do not encode meaning information about the data.

### B.3 Generated samples

The generated samples in Figures 12 to 14 are drawn from models with ConvNets, and Figures 15 to 17 with ResNets.

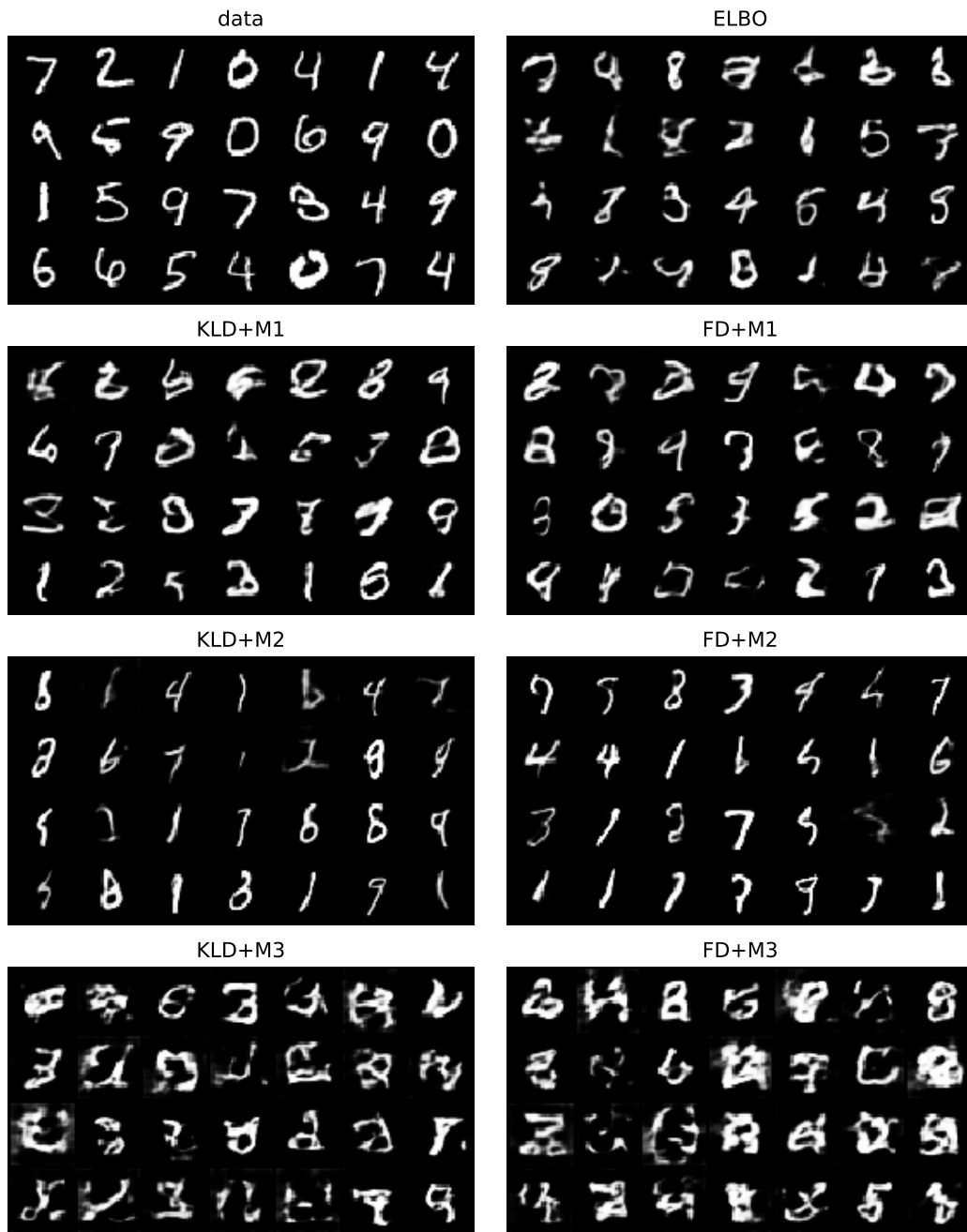


Figure 12: MNIST samples from ConvNet.

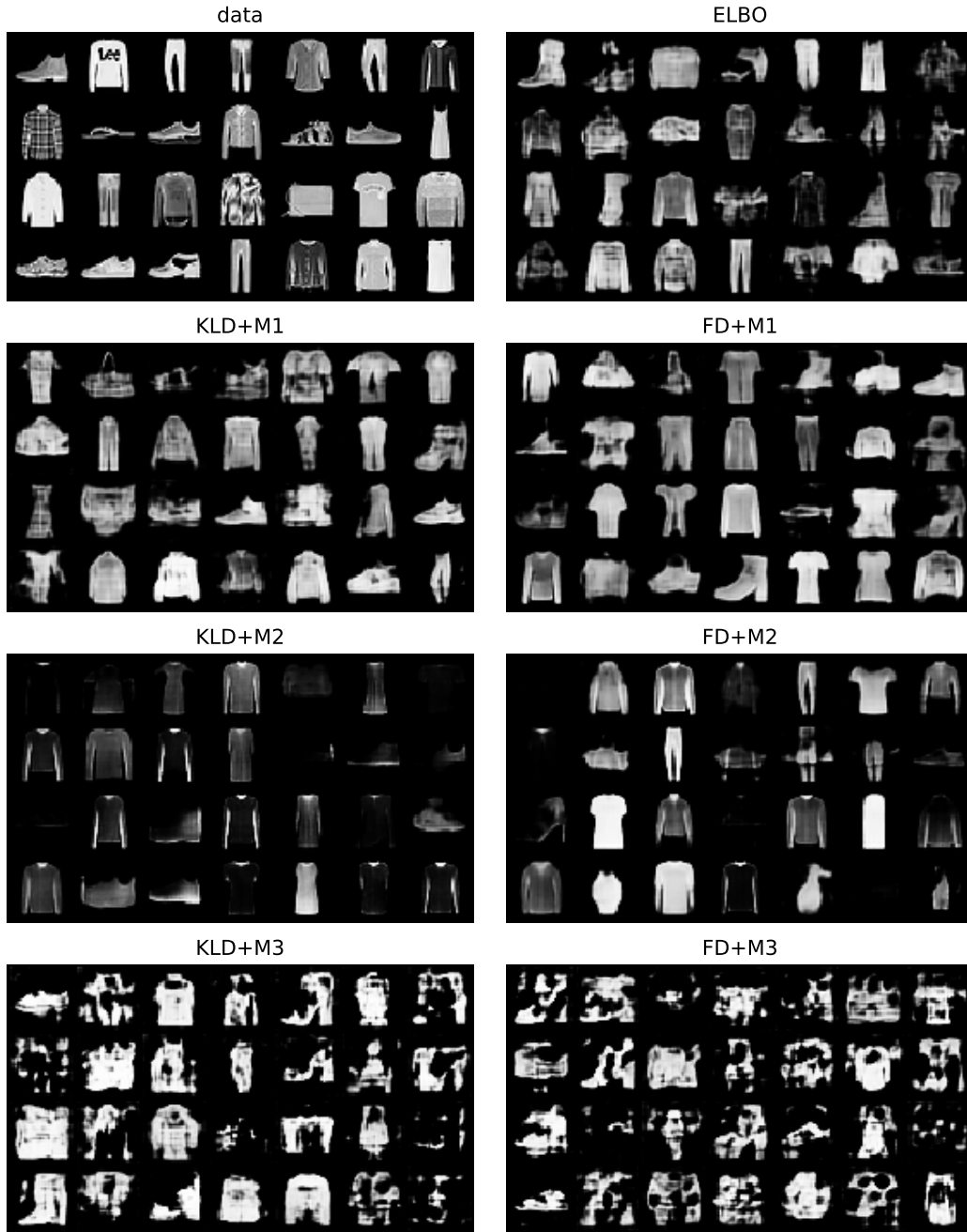


Figure 13: Fashion samples from ConvNet.



Figure 14: CelebA samples from ConvNet.

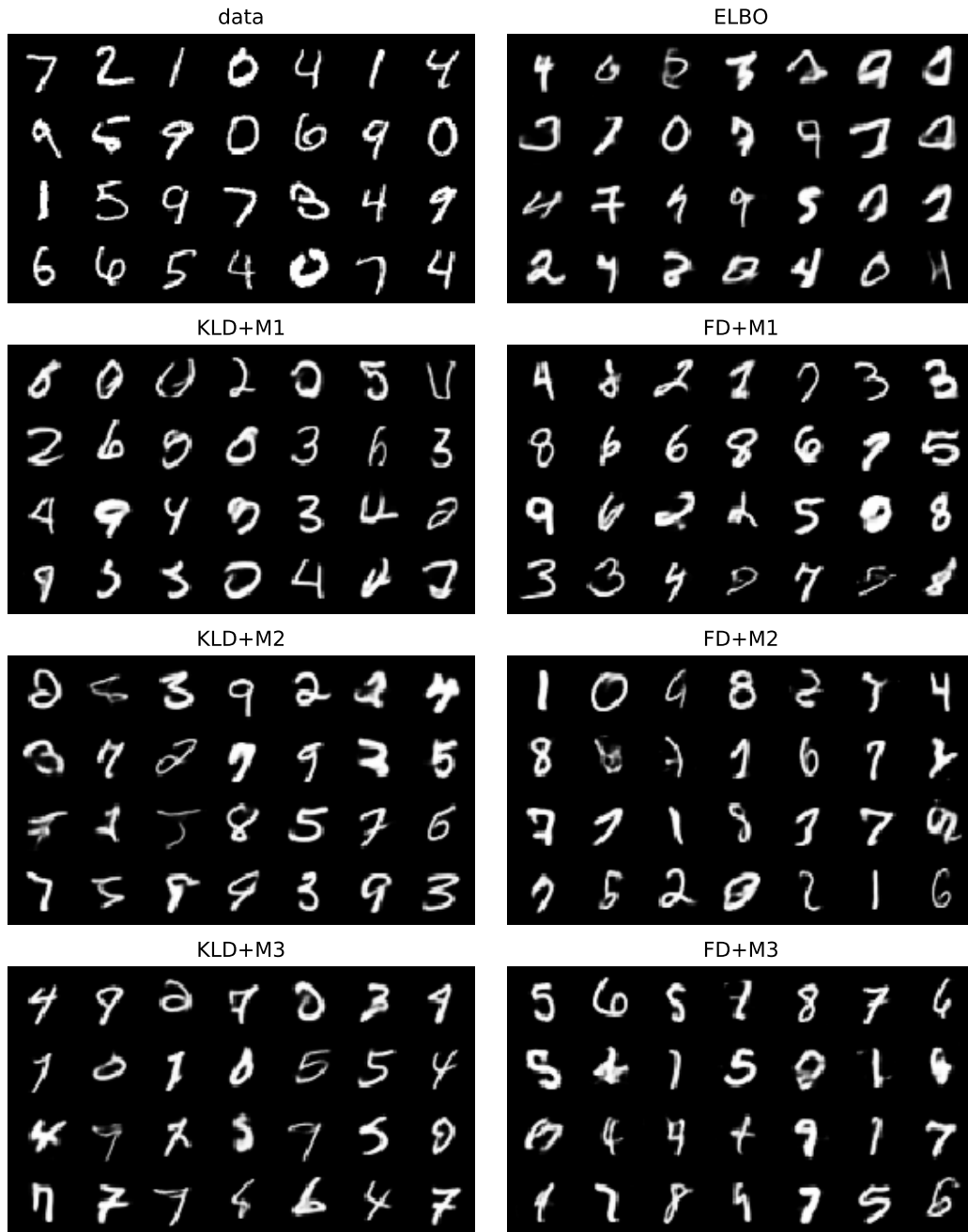


Figure 15: MNIST samples from ResNet.

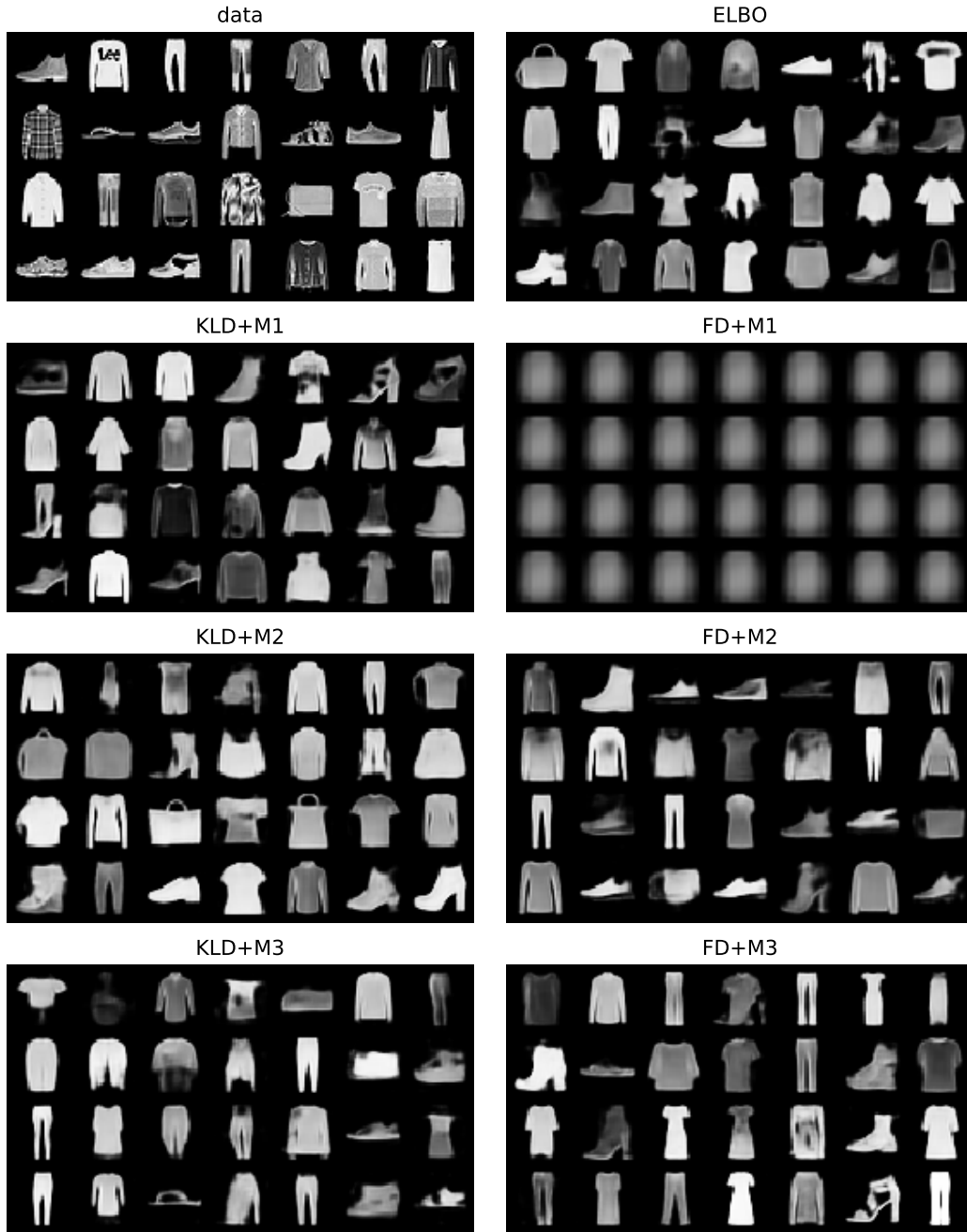


Figure 16: Fashion samples from ResNet.



Figure 17: CelebA samples from ResNet.